1   **Light-absorption of dust and elemental carbon in snow from the Indian Himalaya and**
2   **the Finnish Arctic**

4   Jonas Svensson[1], Johan Ström[2], Niku Kivekäs[1], Nathaniel B. Dkhar[3,4], Shresth Tayal[3,4], Ved P.
5   Sharma[3,4], Arttu Jutila[5], John Backman[1], Aki Virkkula[1], Meri Ruppel[6], Antti Hyvärinen[7], Anna Kontu[8],
6   Henna-Reetta Hannula[8], Matti Leppäranta[5], Rakesh K. Hooda[1,3], Atte Korhola[6], Eija Asmi[1], Heikki
7   Lihavainen[1]

8   [1]Atmospheric Composition Research, Finnish Meteorological Institute, Helsinki, Finland
9   [2]Department of Environmental Science and Analytical Chemistry, Stockholm University, Stockholm,
10   Sweden
11   [3]The Energy and Resource Institute, New Delhi, India
12   [4]The Energy and Resource Institute University, New Delhi, India
13   [5]Department of Physics, University of Helsinki, Helsinki, Finland
14   [6]Department of Environmental Sciences, University of Helsinki, Helsinki, Finland
15   [7]Expert Services, Finnish Meteorological Institute, Helsinki, Finland
16   [8]Arctic Research Center, Finnish Meteorological Institute, Sodankylä, Finland
17
18   *Correspondence to* J. Svensson (jonas.svensson@fmi.fi)

1   **Abstract**

2   Light-absorbing impurities (LAI) deposited to snow have the potential to substantially affect the snow

3   radiation budget, with subsequent implications for snow melt. To more accurately quantify the snow

4   albedo, the contribution from different LAI needs to be assessed. Here we estimate the main LAI

5   components, elemental carbon (EC) (as a proxy for black carbon) and mineral dust in snow from the

6   Indian Himalaya and pared the results to snow samples from Arctic Finland. The impurities are

7   collected onto quartz filters and are analyzed thermal-optically for EC, as well as with an additional

8   optical measurement to estimate the light-absorption of dust separately on the filters. Laboratory tests

9   were conducted using substrates containing soot and mineral particles specially prepared to test the

10   experimental setup. Analyzed ambient snow samples show EC concentrations that are in the same range

11   as presented by previous research, for each respective region. In terms of the mass absorption cross

12   section (MAC) our ambient EC had surprisingly about half of the MAC value compared to our

13   laboratory standard EC (chimney soot), suggesting a less light absorptive EC in the snow, which has

14   consequences for the snow albedo reduction caused by EC. In the Himalayan samples, larger

15   contributions by dust (in the range of 50 % or greater for the light absorption caused by the LAI)

16   highlighted the importance of dust acting as a light absorber in the snow. Moreover, EC concentrations

17   in the Indian samples, acquired from a 120 cm deep snow pit (covering possibly the last five years of

18   snow fall), suggest an increase in both EC and dust deposition, while at the same time proposing a

19   tendency for a reduction in the MAC value with snow depth. This work emphasizes the complexity in

20   determining the snow albedo, showing that LAI concentrations alone might not be sufficient, but

21   additional transient effects on the light-absorbing properties of the EC need to be considered and studied

22   in the snow. Equally imperative is to confirm the spatial and temporal representativeness of these data

23   by comparing data from several and deeper pits explored at the same time.

1   1. **Introduction**

2   The deposition of light-absorbing impurities (LAI) in snow influences the radiation budget and can

3   cause enhanced melting via snow darkening (Warren and Wiscombe, 1980). This process affects

4   regions with seasonal snow cover, leading to an earlier snow retreat, which has major implications for

5   thawing and biogeochemical processes acting in the ground (AMAP, 2011). In mountainous areas with

6   glaciers, the impurities perturb glacier properties and the hydrological cycle (e.g. Xu et al., 2009). The

7   impact on snow reflectance (albedo) from black carbon (BC) aerosol particles is of particular interest.

8   Being one of the most effective light-absorbing aerosols, BC enters the atmosphere by combustion of

9   carbon-based fuels, in activities including forest fires and anthropogenic burning of bio- and fossil fuels

10   (Bond et al., 2013). Because of its negative effect on snow albedo, considerable effort has been made

11   to globally quantify BC in snow (e.g. Doherty et al., 2010; Ming et al., 2008; Schmitt et al., 2015), as

12   well as in ice cores (e.g. McConnell et al., 2007; Ruppel et al., 2014; Xu et al., 2009).

13   The potential impact of LAI in snow and ice make the Himalaya a region of special interest. It contains

14   numerous glaciers which are in a general state of recession, although contrasting patterns have been

15   reported in different areas (e.g. Bolch et al., 2012; Kääb et al., 2012). Himalayan glaciers act as

16   freshwater sources for several major rivers in Asia, including Indus, Ganges, Brahmaputra, Mekong,

17   and Yangtze, thus having a vital part in millions of people's lives (e.g. Immerzeel et al., 2010). The

18   glaciers are especially susceptible to BC emissions, since India and China located in close proximity,

19   emit the most BC world-wide (Bond et al., 2013). A recent study by Ming et al. (2015) found a

20   decreasing trend in albedo during the period of 2000-2011 on Himalayan glaciers, and suggested rising

21   air temperatures and deposition of LAI to be responsible for the decrease. In light of the vast area of the

22   Himalayas, there is a lack of in-situ measurements of LAI on glaciers, which are crucial for modeling

23   work (Gertler et al., 2016). The lack of measurements is especially pronounced in the Indian Himalaya,

24   since previous measurements of LAI in Himalayan snow and ice have largely been confined to China

25   (e.g. Xu et al., 2006) and Nepal (e.g. Ginot et al., 2014; Kaspari et al., 2011; Kaspari et al., 2014; Ming

26   et al., 2008).

27   In addition to BC, other LAI can contribute significantly to the radiative balance of the cryosphere.

28   Recent research has identified mineral dust and microorganisms as having a more important role than

29   previously thought in the current decline in albedo of the Greenland Ice sheet and other parts of the

30   Arctic (e.g. Dumont et al. 2014, Lutz et al., 2016). Similarly, Kaspari et al. (2014) reported such high

31   dust concentrations in the snow of Himalayan Nepal that the contribution of dust in lowering the snow

32   albedo sometimes exceeded that of BC. The importance of dust has also been illustrated from other

33   regions, for example the Colorado Rockies, US, where dust causes a significantly earlier peak in runoff

34   (Painter et al. 2007). In the Arctic, Doherty et al. (2010) suggest that 30 to 50 % of sunlight absorbed

35   in the snowpack by impurities is due to non-BC constituents. Evidently, dust has an important role in

1   the cryospheric radiative balance. Differentiating between the different impurities in the snow is not

2   trivial, however, and requires more than one analytical technique (Doherty et al., 2016). Traditionally,

3   dust in snow has been quantified by gravimetrically measuring filters (e.g. Aoki et al., 2006; Painter et

4   al., 2012). Other methods consist of using transmitted light microscopy (Thevenon et al., 2009), a

5   microparticle counter to measure the insoluble dust (Ginot et al., 2014), or mass spectrometry (using

6   iron as a proxy for dust) (Kaspari et al., 2014).

7   At present, three primary methods are used to measure BC in snow and ice (see Qian et al., 2015, in

8   which they are extensively presented). Out of the three methods, two utilize filters to collect impurities

9   in a melted sample. The first filter method measures optically the spectrally resolved absorption by the

10   impurities using an integrating sphere integrating sandwich spectrophotometer (ISSW) (e.g. Doherty et

11   al., 2010; Grenfell et al., 2011). The second filter method is the thermal-optical analysis of filters (e.g.

12   Forsström et al., 2009; Hagler et al., 2007). The third, non-filter-based method, uses laser-induced

13   incandescence with a single particle soot photometer (SP2) (e.g. McConnell et al., 2007; Schwarz et al.,

14   2012).

15   Each measurement method has benefits and drawbacks. The SP2 is specific to refractory BC and is able

16   to provide estimates on the size of the BC particles. However, the SP2 has a size range limitation

17   (roughly 70–600 nm, depending on the instrument settings and nebulizer setup), which may result in

18   the underestimation of BC mass since particles in snow have been reported to be larger (Schwarz et al.,

19   2012; Schwarz et al., 2013). The use of filters, on the other hand, can provide a practical logistics

20   advantage for the collection of LAI in remote locations because it is difficult to maintain the necessary

21   frozen chain for the snow samples from the field to the laboratory for analysis. Particulate losses can be

22   very significant if a sample is not kept frozen, thus not providing accurate results. Filtering of liquid

23   samples can be conducted in the field, and the substrates are more easily stored and transported to the

24   laboratory. The ISSW method has the advantage that it measures light-absorbing constituents on the

25   filter indiscriminately. Thus, the ISSW method is not specific to BC, and requires interpretation of the

26   spectral response to determine the BC component. The thermal-optical method (TOM) provides an

27   actual measurement of elemental carbon (EC) that is instrumentally defined. EC is assumed to be the

28   dominant light-absorbing component of BC, and often EC and BC are used interchangeably in literature.

29   The sampling efficiency of quartz filters used in TOM is not well characterized for small particles (Lim

30   et al., 2014). However, smaller particles normally contribute little to total particulate mass (Hinds 1999).

31   Thus, each method for measuring BC in snow has both advantages and disadvantages.

32   Here we present observations of LAI in snow from two glaciers in the Sunderdhunga valley in the

33   Indian Himalaya, which have not to our knowledge, been explored previously with respect to LAI in

34   snow. Using a measuring approach whereby the TOM is combined with a custom-built particle soot

35   absorption photometer (PSAP), we perform laboratory tests to provide a correct interpretation of the

1   results. Our Himalayan observations are further compared to samples from Arctic Finland for their LAI

2   content.

3   **2.   Methodology**

4   **2.1 Snow sample collection and site characteristics**

5   *2.1.1 The Indian Himalaya*

6   Snow samples were collected in September of 2015, during the Indian post-monsoon season, from two

7   adjacent glaciers in the Sunderdhunga valley (Figure 1). Bhanolti and Durga Kot glaciers (N 30º 12', E

8   79º 51') are located in the state of Uttarakhand, India. Facing northeast the glaciers cover an elevation

9   range of about 4400-5500 m a.s.l. and are two small valley-type glaciers in the Ganges hydrological

10 basin. Since the glaciers are situated at a relatively low altitude, they are more likely to be exposed to

11 BC than other Himalayan glaciers at a higher altitude, as BC has been shown to decrease with altitude

12 in other parts of the Himalaya (e.g. Kaspari et al., 2014; Ming et al., 2013; Yang et al., 2015). The

13 Sunderdhunga area does not have any major local pollution sources. Regionally, however, the small

14 towns of Bageshwar (~40 km S; population ~9000) and Almora (~70 km S; population ~34000), may

15 play a role. On a larger scale, the Sunderdhunga area is affected by the large-scale emissions from the

16 Indo-Gangetic Plain (IGP). Measurements of airborne BC and other aerosol particles at Mukteshwar, a

17 distance of ~90 km southwards at an altitude of 2200 m a.s.l., have shown a clear seasonal pattern in

18 atmospheric concentrations with emissions originating from the IGP (Hyvärinen et al., 2011;

19 Raatikainen et al., 2017). With a peak during the pre-monsoon season (March-onset of monsoon), the

20 BC loading has been reported to decrease by about 70 % at Mukteshwar during the monsoon (Hyvärinen

21 et al., 2011). Similarly, dust concentrations in the air have been shown to peak during the pre-monsoon

22 season at Mukteshwar (Hyvärinen et al., 2011). The pre-monsoon season, also known as the "dust-

23 season" in India, brings air masses from the Thar Desert transporting dust to the Himalaya (Gautam et

24 al., 2013). Dust from local sources has also been identified at Mukteshwar during this season

25 (Hyvärinen et al., 2011).

26 At Durga Kot glacier four snow pits with varying depths were dug at different elevations, while at

27 Bhanolti glacier one snow pit was dug (see table 1 for snow pits and sample details). Snow samples

28 were collected with a metal spatula in Nasco whirl-pak bags, and thereafter brought to base camp where

29 the snow was melted and filtered. Since it was not possible to maintain the crucial frozen chain for the

30 snow samples during transport back to the laboratory this approach of melting in the field was used for

31 the glacier snow samples. The snow was melted gently over a camping stove in enclosed glassware to

32 avoid contamination. The liquid samples were subsequently filtered through quartz fiber filters

33 (Munktell, 55 mm, grade T 293), in accordance to previous work (e.g. Forsström et al., 2009; Svensson

1 et al., 2013). Filters were dried in ambient conditions in petri dishes and thereafter transported to the

2 laboratory for analysis (described in section 2.2).
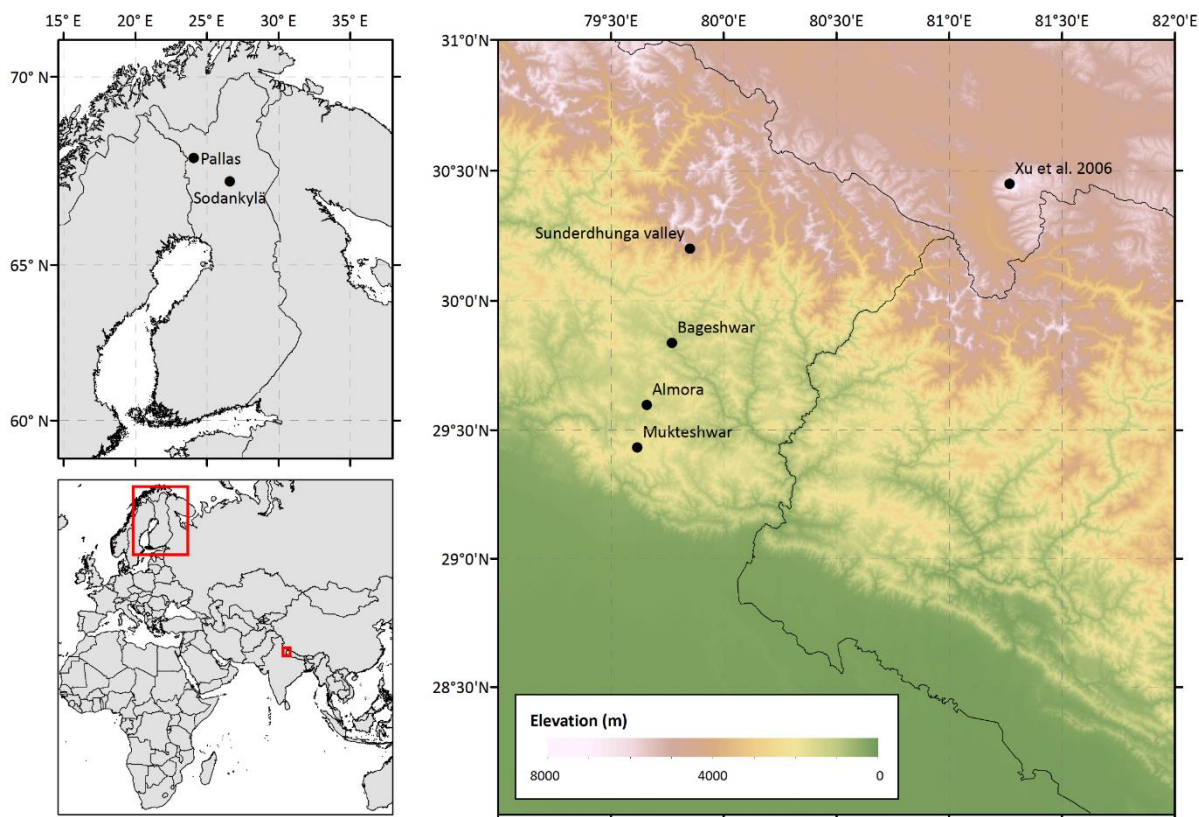
4 Figure 1. Map of sampling locations and sites discussed in text.

5 *2.1.2 Arctic Finland*

6 Snow samples collected in Finland originated from the seasonal snowpack of Sodankylä (N 67º 21' E

7 26º 37') and Pallas (N 67º 58' E 24º 06') c.f. Figure 1. The Pallas samples were gathered in March and

8 April of 2015 (n=10) from an open mire and in March of 2016 (n=2) from an area above the tree line

9 (in close proximity of the Pallas Global Atmosphere Watch Station). More details of the Pallas sampling

10 area are provided in Svensson et al. (2013) where EC in the snow was previously investigated. The

11 sampled snow was confined to the top layers of the snowpack. The Sodankylä samples (n=15) are from

12 the Finnish Meteorological Institute Arctic Research Center, where weekly surface snow samples (0-5

13 cm) have been collected since 2009 (the first part of time series is presented in Meinander et al., 2013;

14 where details of the area are provided). The samples used in this study originate from spring of 2013

15 and 2014. The snow samples from Pallas and Sodankylä were collected in Nasco whirl-pak bags and

16 stored in a frozen state until filtration. Samples were then melted in a microwave oven at each site's

17 respective laboratory, and followed the same filtering procedure described above, according to e.g.

18 Forsström et al. (2009) and Svensson et al. (2013).

1   **2.2 Light-absorbing impurities analysis**

2   To estimate the contribution to the reduction in transmission on the filter sample substrate due to

3   minerals, we compared the light transmission through the filter using the PSAP before and after heating

4   the sample as part of the TOM analysis. Since it is difficult to gravimetrically determine the dust content

5   on quartz filters, we decided to use this combined instrument approach to estimate the dust content. A

6   custom built PSAP (Krecl et al., 2007) was used for the optical measurements, and for the TOM a

7   Sunset Laboratory OCEC-analyzer was used to determine EC. A brief description of the OCEC-

8   analyzer and the PSAP is given below in sections 2.2.1 and 2.2.2, respectively.

9   The approach of measuring light transmission before and after heat treatment to estimate the different

10   light-absorbing components has been previously used for airborne sampled aerosol (e.g. Hansen et al.,

11   1993). In Hansen et al. (1993), filter samples were optically analyzed before and after being treated in

12   a 600ºC furnace, in which the carbonaceous material was vaporized from the filter. These measurements

13   enabled them to obtain an estimate of the dust content on the filter. Lavanchy et al. (1999) followed a

14   similar optical and thermal approach to determine the BC and dust content of ice core samples. For the

15   EC measurement they used a two-step combustion procedure by Cachier et al. (1989), and in between

16   the thermal treatment they used a modified version of an aethalometer to measure the attenuation of

17   light through the filter. Our experimental method is analogous to that of Lavanchy et al. (1999).

18   However, as a Sunset Lab. OCEC-analyzer and a custom built PSAP were readily available to us, this

19   instrument configuration was used in our study. Because results from this type of analysis may be very

20   instrument specific, a series of laboratory tests (described in section 2.3) were conducted to confirm

21   reliability of the method before ambient snow samples were measured. The analysis procedure for the

22   filters (outlined further in section 2.3) was the same for the laboratory samples and the ambient samples.

23   *2.2.1 Elemental carbon analysis*

24   From a 10 cm^2 filter sample area, separate punches of 1 cm^2 were taken and analyzed for organic carbon

25   (OC) and EC content using a Sunset laboratory OCEC-analyzer (Birch and Cary, 1996) with the

26   EUSAAR_2 analysis protocol (Cavalli et al., 2010). First, in a helium atmosphere, the filter punch is

27   heated at different temperature steps. In this phase OC is volatilized and detected by a flame ionization

28   detector (FID). During the second stage, oxygen is introduced, and EC is released from the filter through

29   combustion. To account for pyrolysis (darkening of the filter) occurring during the first step, a laser (at

30   a 632 nm wavelength) measures the transmittance (or reflectance as an option for newer instruments)

31   continuously of the filter punch, and when the original value of the transmittance (measured before

32   thermal sequence starts) is attained during the second step separation between OC and EC is done. The

33   EC values reported here (referred to as EC_{TOM}) are based on the transmittance correction for pyrolysis

34   since the PSAP operates also on the basis of transmittance through the substrate. An additional EC value

35   provided by the OCEC-analyzer from the analysis is an optical EC ($EC_{optical}$), which is based on the

1   monitored transmittance and absorption coefficients of the OCEC-analyzer. Carbonates may be present

2   in filter samples (Chow & Watson, 2002), and unless chemically removed before analysis, these

3   particles will contribute to the OC fraction of the total particulate carbon content in the EUSAAR_2

4   protocol (Cavalli et al., 2010). For our samples, carbonates are assumed to be present in insignificant

5   amounts since our visual inspection of the thermograms from analysis revealed no carbonate peak.

6   Recent tests by Zhang et al. (2017), on acidified and non-acidified filter samples with snow from Tibet

7   have showed less than 20 % discrepancy between treated and non-treated filter substrates.

8   Uncertainties associated with the TOM method are mainly associated with uneven filter loading, ~~and~~

9   loss of particles to filtering containers, and the inefficiency of the filters to capture the impurities

10   (undercatch) (Forsström et al., 2013; Lim et al., 2014). For our filtering set-up the undercatch has been

11   estimated to ca. 22 % (Forsström et al., 2013), and is most likely significant for smaller sized particles,

12   since undercatch tests have indicated an inefficiency for smaller sized particles (Lim et al., 2014).

13   During OCEC-analysis, an artifact from samples with a high fraction of pyrolysis OC (Lim et al., 2014),

14   and the interference of an accurate split point determination from filters containing a high dust load can

15   also be considerable for the TOM method (Wang et al., 2012).

16   *2.2.2 Absorption measurements*

17   The PSAP uses a single diode at 526 nm as light source. The light is split by two light pipes which

18   illuminate two areas of 3.1 mm in diameter. The filter substrate is placed over these areas and individual

19   detectors below the filter measure the transmitted light. During normal operations, when measuring BC

20   in air, these two signals are used as sample and reference spots. The reference spot is exposed to particle

21   free air and the sample spot is exposed to particles present in the ambient air. In this experiment both

22   signals are used to measure the change in transmission by comparing the signal before and after the

23   filter has been analyzed using TOM. The signal change is related to the transmission from a particle

24   free filter (filtered using Milli-Q (MQ) water and dried; the measurement procedure is further explain

25   in 2.3).

26   The corrections required for the PSAP when used for air sampling is well documented (e.g. Bond et al.,

27   1999; Virkkula et al., 2005), in particular this concerns enhanced absorption from the filter itself through

28   multiple scattering effects from the filter fibers, and particle loading effects (shadowing and reduction

29   in multiple scattering). However, these corrections are essentially uncharacterized for melted snow

30   samples and the quartz fiber filters used. The fiber filters used are substantially thicker compared to

31   what is normally used for PSAP measurements (Pallflex cellulose membrane filter) or the ISSW

32   measurements (Nuclepore filter). Moreover, the filter substrate is very large in terms of surface area

33   compared to the particles sampled. The geometry is very complex and in relation to a particle the

34   substrate is more of a three dimensional web or sponge rather than a flat surface area on a filter. An

35   example of a blank filter sample obtained by a scanning electron microscope is presented in Figure 2.

1   The horizontal scale of 500 µm is for comparison, and the scale of 150 µm is to illustrate the relative

2   thickness of the substrate.
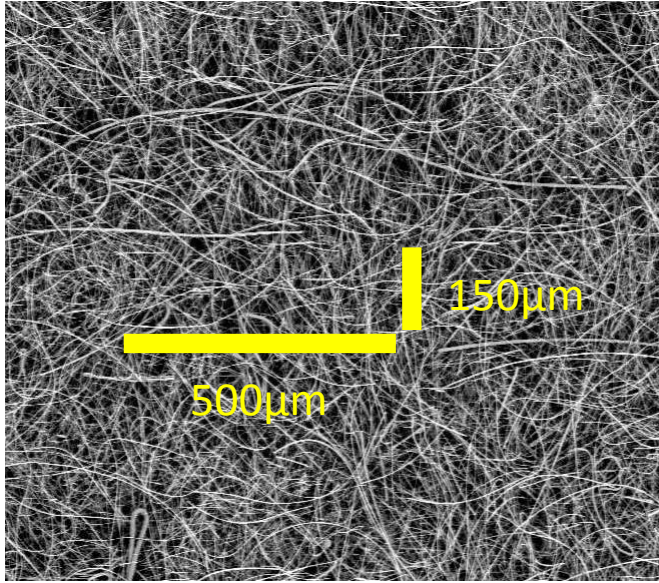
4   Figure 2. Electron microscope image of a blank quartz fiber filter used in this study.

5   The basis for the optical attenuation measurements is the exponential attenuation of light as it passes

6   through some medium, often described by the Bouguer-Lambert-Beer-law (Eq. 1).

$$I = I_0\, e^{-\tau}, \qquad \text{(Eq. 1)}$$

8   where I_0 in our case is the light intensity through a clean filter and, I is the light intensity through a

9   sample loaded filter. The exponent τ is the optical depth of LAI on the filter. For our study the multiple

10   scattering absorption enhancement factor of the filter will be treated as a constant, but not given a

11   numerical value. Due to the geometry of the filter, corrections for any enhanced absorption due to co-

12   existing scattering particles, and the loading effect, are not specifically considered. Hence, we will

13   assume a linear relation between the logarithmic change in transmittance (T_r) of a filter and the optical

14   depth (Eq. 2).

$$ln(T_r) = \tau_{TOT}, \text{ (Eq. 2)}$$

16   where $T_r = \frac{I_0}{I}$ and τ_{TOT} is the combined effect of all light absorbing impurities. Our interest was to

17   estimate the relative contributions of EC (τ_{EC},) and mineral dust (τ_D) particles to measured optical depth

18   according to equation 3.

$$\tau_{TOT} = \tau_{EC} + \tau_D, \text{ (Eq. 3)}$$

20   From TOM we get the EC mass surface density (µg cm^{-2}). Thus, we can write τ_{EC} as the product of the

21   EC mass surface density on the filter and an effective material specific mass absorption cross section

1   $MAC_{eff,EC}$ of BC that includes the multiple scattering enhancement of the filter, which is applicable for

2   our measurements and not necessarily as universal MAC values. Typically, MAC values are reported

3   in units of $m^2 \ g^{-1}$.

4   **2.3 Laboratory tests**

5   A series of laboratory tests using the OCEC-analyzer and the PSAP combination were conducted before

6   initiating analysis of the field samples. For this purpose, the following filter sets were created:

7   1. A set of filter samples (n=36) with different amounts of BC. Two types of soot (BC) were used

8   and each was mixed (a small amount of soot not weighed) with MQ water and a small amount

9   of ethanol (to enable mixing of the BC particles in the liquid) in an ultra-sonic bath. One soot

10   type was collected by chimney cleaners in Helsinki, Finland, originating from oil-based

11   combustion, and has been used previously in soot on snow experiments (Svensson et al., 2016).

12   The second type was a product from NIST (National Institute of Standards and Technology),

13   which consists of diesel particle matter from industrial forklifts, NIST-2975. From the BC stock

14   solutions, different amounts of solution were taken out and diluted with additional water for the

15   same total volume of filtrate (ca. 0.5 L liquid). The newly created mixture solution was

16   thereafter filtered using the same filter procedure as the ambient snow samples (described in

17   2.1.1).

18   2. The second set of filters (n=16) generated contained mineral dust only. Analogous to the soot

19   mixtures, two types of mineral were used. The first mineral was SiC, (manufactured by

20   Carborundum), mesh nr. 1200, corresponding to particles approximately < 1 μm in diameter

21   (Manufacturer). It is light grey with hints of blue in color and the amount of SiC added to the

22   MQ water was measured using a digital scale (resolution of 10 μg) before filtration. With the

23   known concentration of the mixture, we observed how much of the weighed mineral was

24   deposited on the filter during filtration to estimate losses. By comparing the whole filters before

25   and after filtration gravimetrically, these tests showed that 10 % or less of the mineral was lost

26   during filtering. The second type of mineral consisted of stone crush from a site in Stockholm,

27   Ulriksdal, likely to be mainly granite. A sieve mesh nr. 400 was used for this material, which

28   corresponds to mineral particles of approximately < 38 μm in diameter. Filters were prepared

29   according to the procedure given above for the other mineral (SiC).

30   3. The last set of laboratory solutions made contained various mixtures of SiC mineral and

31   chimney soot (n=30). These filters were treated in the same way as described above, with a soot

32   stock solution and a mineral weighed solution being mixed into one solution.

33   The procedure to analyze all three sets of filters samples was identical. After the filter substrates had

34   dried, one punch (1 cm^2) from the filter was put into the PSAP instrument to measure the transmission

1   across the filter in relation to a blank filter. This punch was taken for analyses of OC and EC content

2   using the OCEC-analyzer. After the TOM, and removal of the carbonaceous particles, this filter punch

3   was again analyzed in the PSAP. Hence, we acquired the transmission through the filter before heating

4   and after heating in comparison to a blank filter. We did tests where the same filter punch was used in

5   the PSAP instrument as well as the OCEC-analyzer, and compared this to identical samples that were

6   used only in each instruments. Both procedures provided the same result. Furthermore, extensive tests

7   were carried out using blank filters that had been subject to filtering of MQ water and treated the same

8   way as prepared samples and the ambient snow samples. No measurable EC could be detected on these

9   filters. It should be noted that part of the second set of the laboratory filters (stone crush mineral) were

10   analyzed with a different, but identical, PSAP and OCEC-analyzer at a different laboratory (Stockholm

11   University).

12   **3.   Results and discussion**

13   **3.1 Laboratory samples**

14   The change in optical depth as a function of analyzed EC using our two standard types of BC particles

15   (filter set nr. 1) is shown in Figure 3. Both materials behave optically similar and the slopes are within

16   15 % of each other, with chimney soot having a slope of 39.8 ± 1.5 m^2 g^{-1} and NIST soot 34.4 ± 1.8 m^2

17   g^{-1} (fits have been set to a fixed intercept at 0; $\pm$ refers to standard error of slope). Previous studies of

18   atmospheric airborne BC aerosol and its MAC with different filter-based absorption photometers are

19   numerous, while reported MAC values for BC in snow are very sparse. The MAC value of BC is

20   dependent on many factors, such as particle size, density, and refractive index, mixing state (i.e.

21   coating). Reported airborne BC MAC values are lower than what we found for the two soot standards

22   (which were mixed in liquid solution to simulate similar conditions as for our ambient snow samples).

23   However, the MAC of air sample usually takes into account the multiple-scattering correction factor

24   (C_{ref}). For example for the commonly used aethalometer, its optical depth is divided by a C_{ref} in the

25   range of 2.8-4.3 (Collaud Coen et al., 2010). If a C_{ref} of 5.2 was considered for our BC solution data,

26   similar MAC values would be found (e.g. Bond et al. (2013) reports freshly-generated BC with a MAC

27   of 7.5 ± 1.2 m^2 g^{-1} at $\lambda = 550$ nm). However, for our data set we have chosen not to take any C_{ref} into

28   account as our samples are liquid instead of air based, and currently no C_{ref} exists for liquid samples.
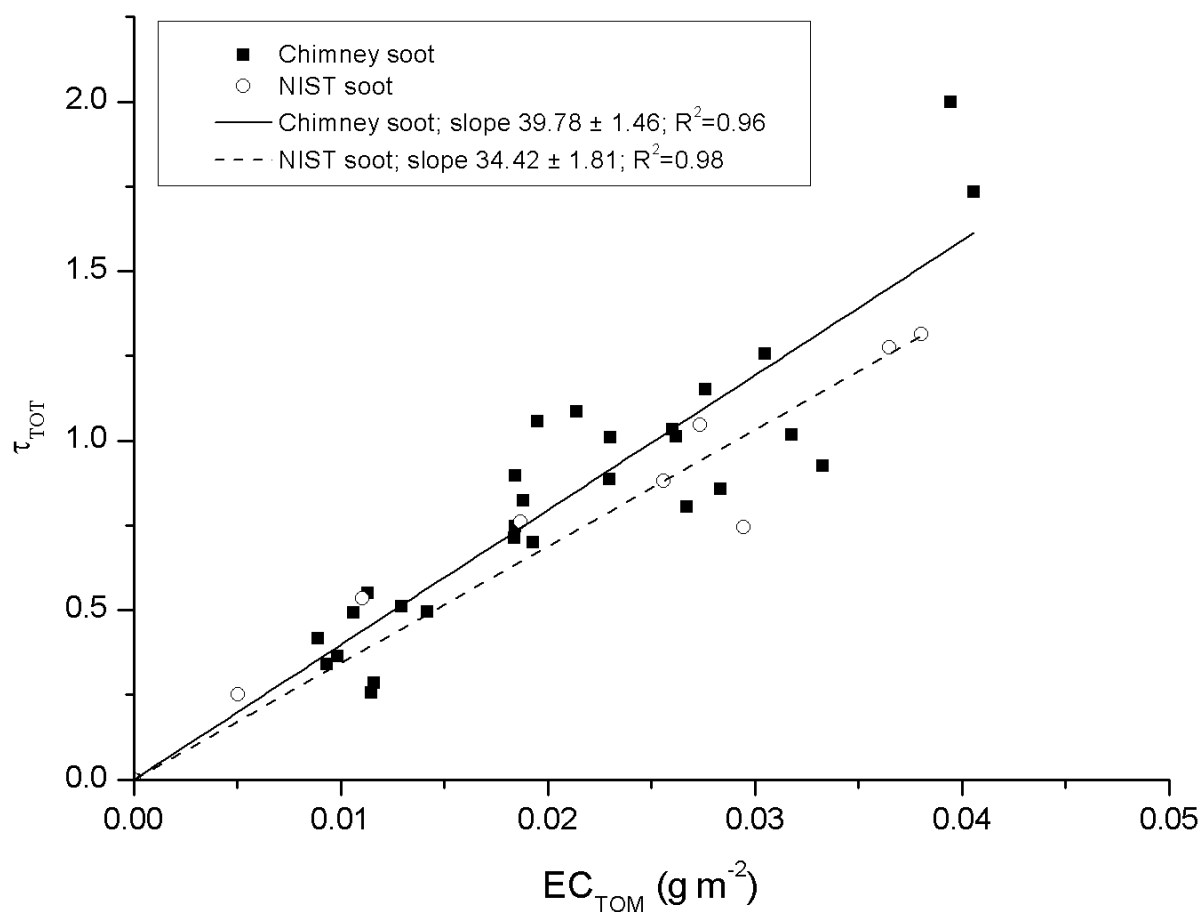
3   Figure 3. Comparison of the optical depth (at λ=526 nm) by Chimney and NIST soot as function of

4   analyzed EC density by the OCEC-analyzer.

5   Figure 4 shows results analogous to Figure 3, but for the two mineral aerosol solutions (filter set nr. 2).

6   The slope of the optical depth of SiC versus measured SiC amount is more than a factor of one hundred

7   smaller (0.23 ± 0.008 m^2 g^{-1}) than the slopes for our BC standards. This is consistent with previously

8   reported results for airborne mineral dust (e.g. Hansen et al., 1993). The stone crush material, an

9   essentially white powder, yielded an even smaller slope of 0.02 ± 0.001 m^2 g^{-1}. Clearly, the slopes, or

10   the MAC, for the mineral particles are very composition specific. For a few (n=5) of the mineral aerosol

11   samples the optical depth was measured both before and after TOM. No EC was detected on these

12   samples and no significant difference in τ could be observed before and after heating the sample, as one

13   would expect since no BC was added to these filters.
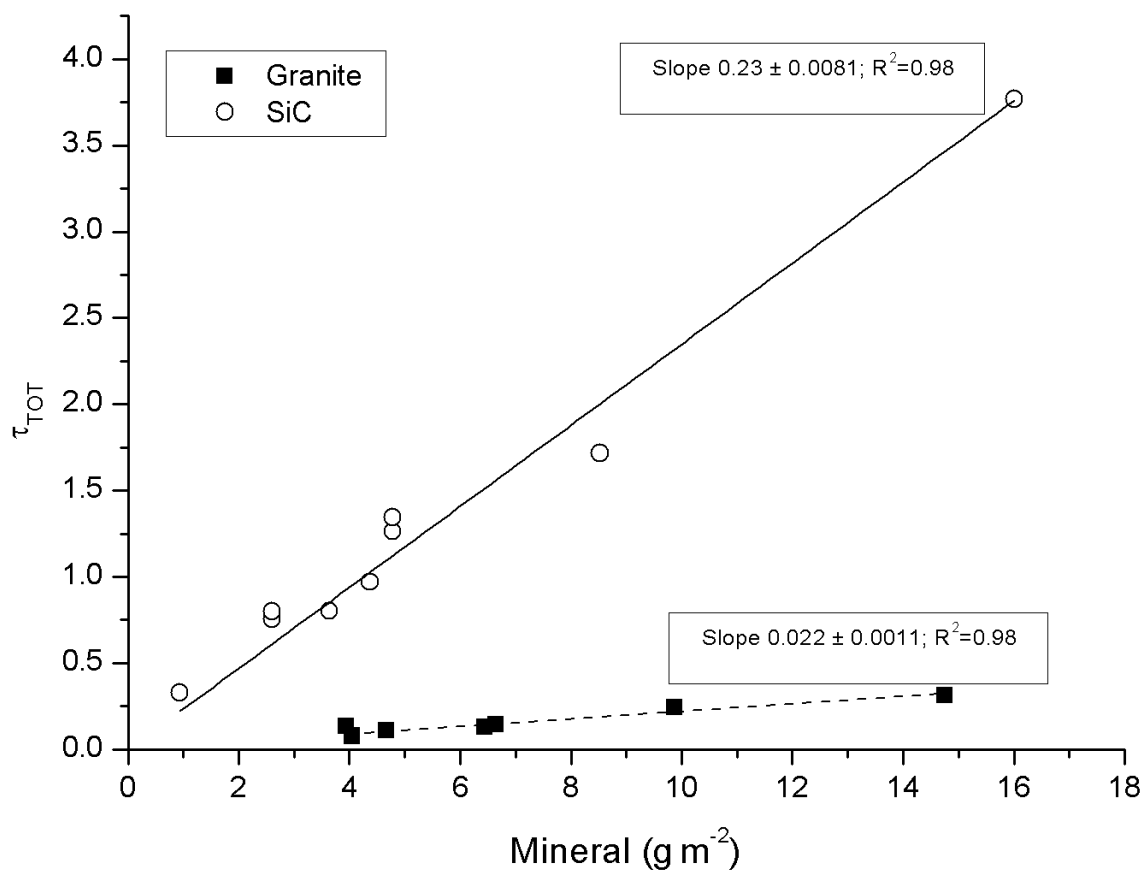
2 Figure 4. The optical depth (at λ=526 nm) as a function of the amount of minerals present on the filter.

3 From the analysis of chimney and NIST soot (Fig. 3) and SiC and stone crush dust (Fig. 4) the

4 experiments were extended to comprise mixtures of soot and dust. Using the MAC of chimney soot

5 (see Fig. 3), we estimate the EC content of the third set of filters, containing a mixture of SiC and

6 chimney soot. The estimated EC (eEC) is based on the difference between the optical thickness before

7 TOM analysis (τ_{TOT}) and the optical thickness after the analysis (τ_D). eEC is then compared to the

8 amount of EC obtained in TOM, for the same filters. This comparison is presented in Figure 5. The data

9 are rather scattered, but the slope of the linear regression is within 17 % of the 1:1 line. Hence it shows

10 that EC can be reproduced reasonably well based on the PSAP measurement even for a mixture of BC

11 and minerals.
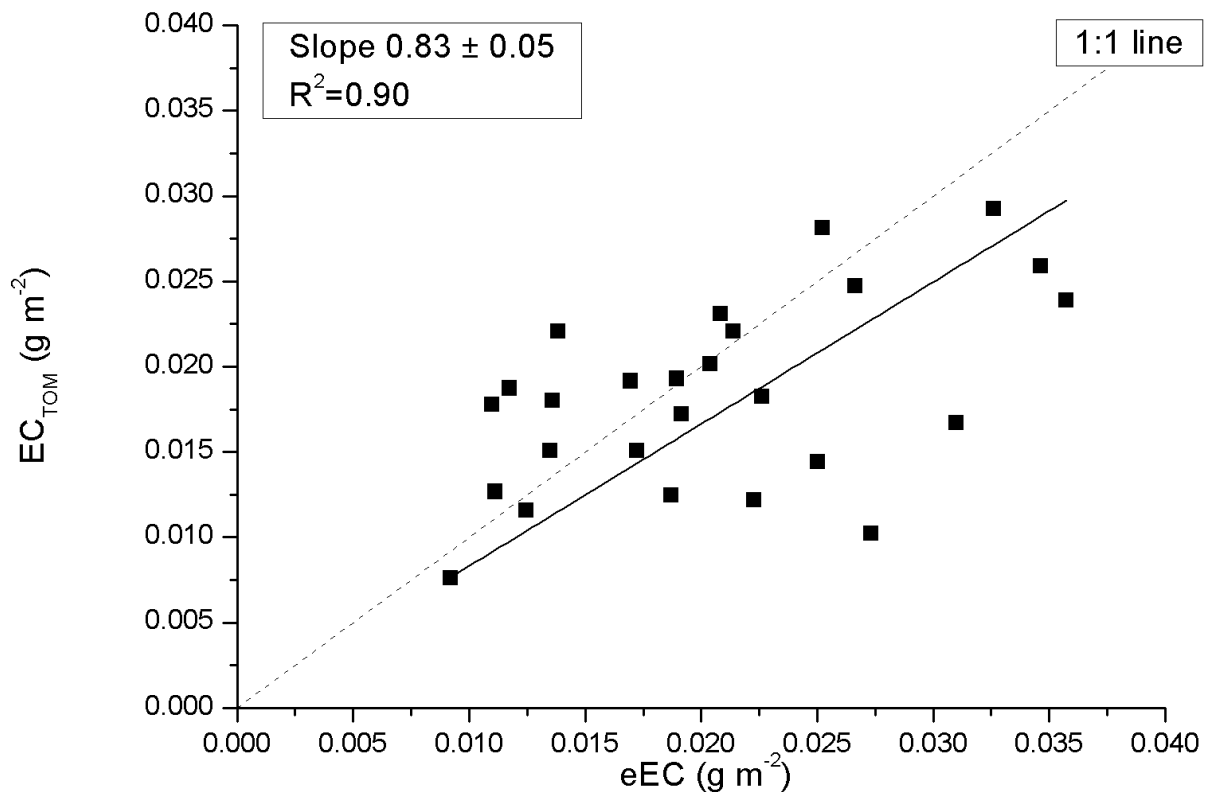
2 Figure 5. EC amount observed by the TOM (EC_{TOM}) for Chimney soot and SiC mixtures as a function

3 of estimated EC (eEC), using a PSAP optical depth signal before and after heating the filter and using

4 the $MAC_{eff,EC}$ of 39.8 m^2 g^{-1} from Figure 3.

5 In the context of this work it is further useful to compare our eEC content with the optical EC reported

6 by the OCEC-analyzer. This comparison is presented in Figure 6, again for the third set of filters

7 (Chimney soot+SiC). As observed, the EC amounts derived by two optically different methods show a

8 consistent relation with nearly a slope of one. The good agreement between the two optically derived

9 EC values suggests that much of the scatter seen in Figure 5 is due to the difference in the detection

10 techniques (optical vs. TOM). The observed scatter in Figure 5 could also be related to the fact that BC

11 is mixed with SiC.
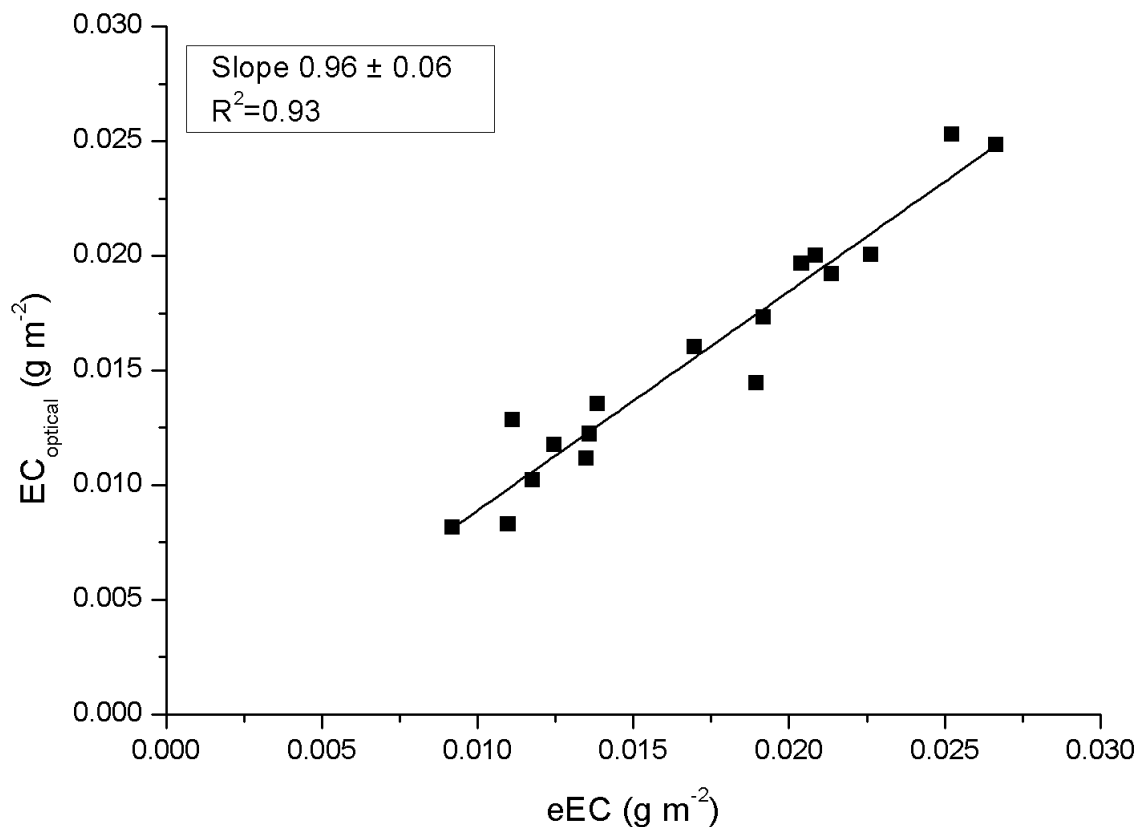
2   Figure 6. Comparison between the optical~~ly~~ measurement of ~~reported~~ EC by the OCEC-analyzer and

3   the derived EC surface amount on the substrate ~~(~~using PSAP data and the relation in Figure 3~~)~~. The data

4   is for filters containing mixtures of Chimney soot and SiC.

5   In addition to chimney soot, the mineral SiC is the second absorbing component on the third set of

6   filters. In Figure 7 the optically estimated SiC content, based on the SiC slope in Figure 4 and τ_D is

7   compared to the known weighed amount of SiC before adding it to the liquid. Similarly, as in Figure 5,

8   there is some scatter in the data, but the overall pattern indicates a consistency with a reliable optical

9   measurement. Two slopes presented, one including all of the data points (slope 1.02), and the second

10   slope (0.88) excluding three data points with weighed SiC amounts exceeding 7.5 g m^{-2}.
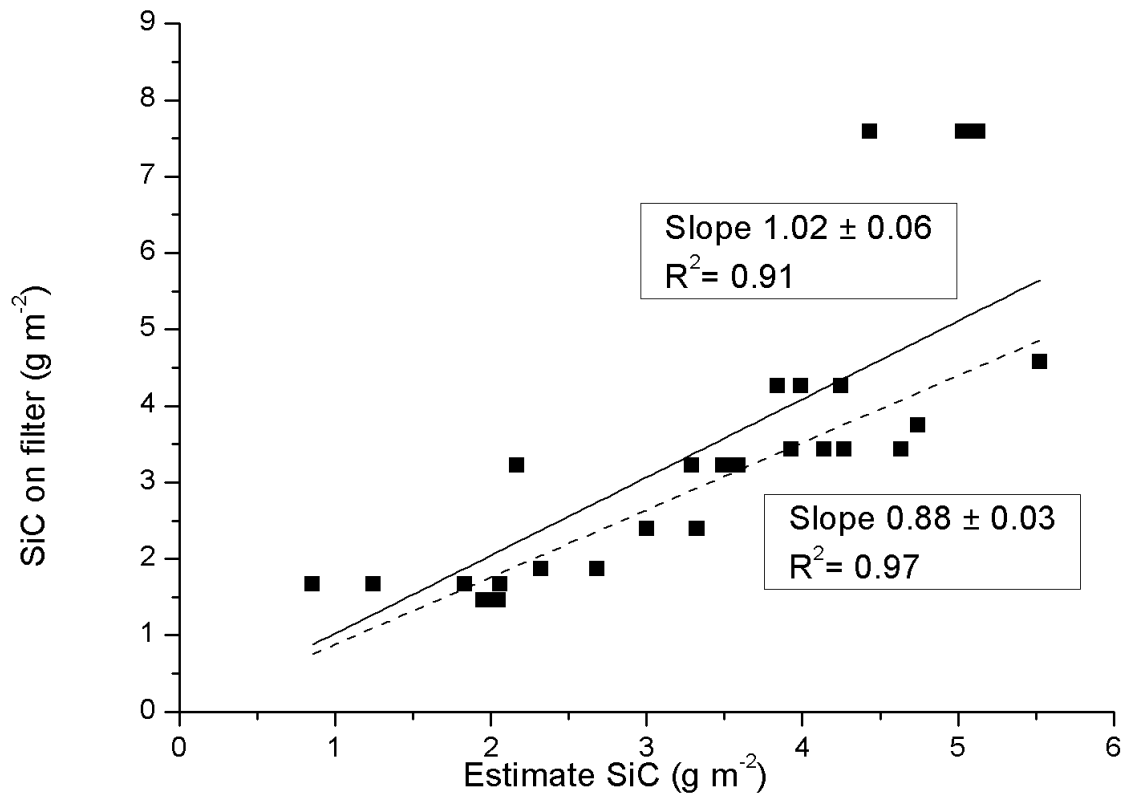
2 Figure 7. Comparison between the weighed SiC amounts added to the water and the optically derived

3 SiC density on the substrate. The data is for Chimney soot and SiC mixtures, with two alternative slopes;

4 one containing all data points (1.02), and one excluding three data point in the top right of graph (0.88).

5 Based on the relations established for EC and SiC individually in figures 3 and 4, respectively, it is

6 possible to retrieve their separate concentrations from a mixture based on the change in filter

7 transmission before and after heating the filter. The consistent results from these laboratory tests gives

8 confidence in applying this method on our ambient samples from India and Finland.

9 **3.2 Ambient snow samples**

10 *3.2.1 EC in snow*

11 In all of the snow pits from Sunderdhunga a distinct layer with concentrated impurities was observed.

12 These impurity layers always had the highest EC concentrations (exceeding 300 µg L^{-1}) of each pit

13 (Table 1). For some of the samples from Sunderdhunga taken from the impurity concentrated layers,

14 the substrates were actually too loaded with material and quantitative impurity values could not be

15 determined (by not having an initial transmission value). Excluding these heavy impurity layers, the

16 average and median EC concentration for the other snow samples were 141.3 and 101.9 µg L^{-1},

17 respectively. Surface samples taken above 4900 m a.s.l. had EC concentrations in the range of 13.2-

1   65.7 µg L^{-1}. Consisting of relatively fresh snow, fallen during the previous days (or weeks), these

2   surface samples contained LAI mostly originate from the post-monsoon season.

3   Previous studies of BC in snow and ice from the Himalaya have shown seasonal variation. At Mera

4   glacier in Nepal Ginot et al. (2014) showed that BC concentrations peak during the pre-monsoon in a

5   shallow ice core. From the same glacier, Kaspari et al. (2014) observed similar seasonal peaks in BC

6   concentration in snow and firn samples taken above the equilibrium line altitude, where the snow had

7   not undergone any significant summer melt. Noteworthy, dust did not show the same strong seasonality

8   as BC in their studies (Ginot et al., 2014; Kaspari et al., 2014).

9   Measurements of BC in snow taken closest to Sunderdhunga, reported in the literature, are from about

10   140 km east-north-east (78º heading), at a higher altitude between 5780-6080 m a.s.l. Gathered in the

11   surface snow of Namunani glacier Xu et al. (2006) reported low EC concentrations in the range of 0.3-

12   9.7 µg L^{-1}. The difference between Sunderdhunga and Namunani can probably be attributed to the

13   expected high spatial variability of BC in snow in the area. The difference in sampling altitude and

14   different measurement techniques to determine the EC likely plays a role as well (Xu et al. used a two-

15   step heating-gas chromatography, similar to method of Lavanchy et al.). The difference could also

16   possibly be explained by the geographical location, with Namunani located on the northern flank of the

17   Himalaya, and it is on the leeward side of the main sources of LAI to the south. Furthermore, it is not

18   explicitly stated in Xu et al. during which season snow samples were collected, which likewise would

19   affect EC concentrations.

20   For reference, the EC concentration in the surface snow from the Finnish Arctic were in the range of

21   6.2-102 µg L^{-1}. Samples from Pallas had an average and median of 40.0 and 31.0 µg L^{-1}, respectively,

22   whereas the samples from Sodankylä had an average of 23.7 µg L^{-1} and median of 13.1 µg L^{-1}. The

23   higher concentration observed in Pallas might result from the fact that the majority of samples was

24   taken later in the snow season compared to Sodankylä samples and EC has likely concentrated in the

25   surface snow later in the season (e.g. Svensson et al., 2013). On a larger scale, the concentrations are in

26   the same magnitude as previous measurements of EC in snow from the European Arctic (Forsström et

27   al., 2013; Meinander et al., 2013; Svensson et al., 2013).

28   Our snow samples EC content is further compared in Figure 8, where the estimated EC content based

29   on the optical depth measurement is plotted against the optical EC output from the OCEC-analyzer. The

30   snow data presented in Figure 8 indicate the same relation between the two optical methods as presented

31   in Figure 6 for the standard soot. That is, slopes near 1:1 line, namely 1.19, 1.02, and 1.11 for

32   Sunderdhunga, Pallas, and Sodankylä samples, respectively. Hence, there is a strong consistency

33   between the two optical approaches in the interpretation of the change in τ before and after the substrate

34   has been analyzed with the EUSAAR-2 thermal protocol.
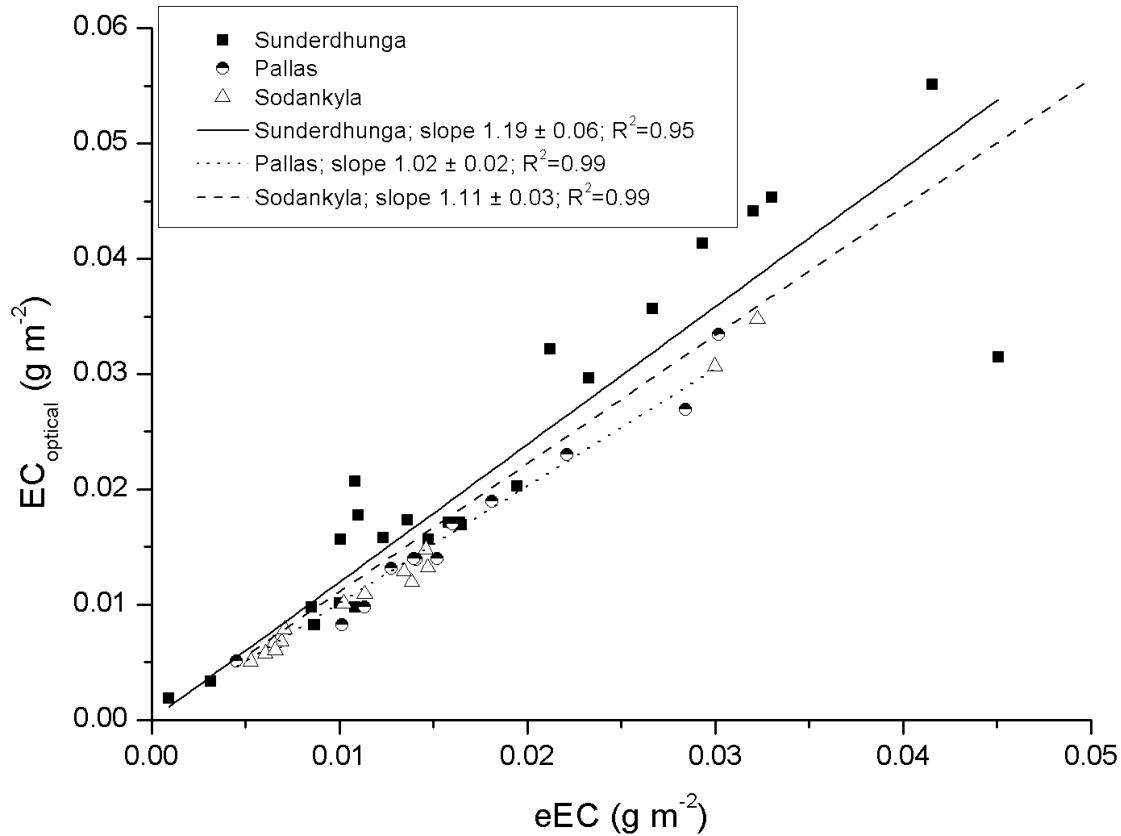
2 Figure 8. Comparison between the optical EC content given by the OCEC-analyzer and estimated EC

3 (eEC) content using a PSAP and a $MAC_{eff,EC}$ of 39.8 m^2 g^{-1}, for the Arctic and Himalayan samples.

4 Although the EC content determined by the optical method of the TOM and the eEC content based on

5 the PSAP and a MAC value (Figure 3) agree well, there is a significant difference in the site specific

6 derived MAC values. In Figure 9 the optical depth of EC (τ_{EC}) is plotted as a function of the analyzed

7 EC (with TOM) for all of the snow samples. The slopes for the three sampling sites are 21.0, 21.9 and

8 17.1 m^2 g^{-1} (Pallas, Sodankylä, and Sunderdhunga, respectively). These values are around half of what

9 the laboratory standard BC tests show (Fig. 3), indicating a smaller absorption efficiency for the EC

10 particles originating from the snow compared to the laboratory particles. This is unexpected, as any

11 non-EC absorbing material or even scattering particles mixed with EC would tend to increase the MAC

12 value compared to pure BC particles (e.g. Cappa et al., 2012; Bond et al., 2013). In our case, we would

13 expect the MAC to be greater for our snow originating EC particles. A consequence of a lower MAC

14 for the snow EC particles could be that the snow albedo reduction caused by the EC is inaccurate since

15 the EC particles have less absorbing efficiency. Schwarz et al. (2013) previously reported a lower MAC

16 value for BC particles in the snow compared to airborne BC particles due to a difference in the measured

17 mean size. The BC particles from the snow were observed to be larger compared to airborne BC

18 particles, explaining the decrease in MAC for the snow particles. The authors further showed how the

1   BC effect in snow albedo reduction is currently overestimated due to the lower MAC for snow BC

2   particles.
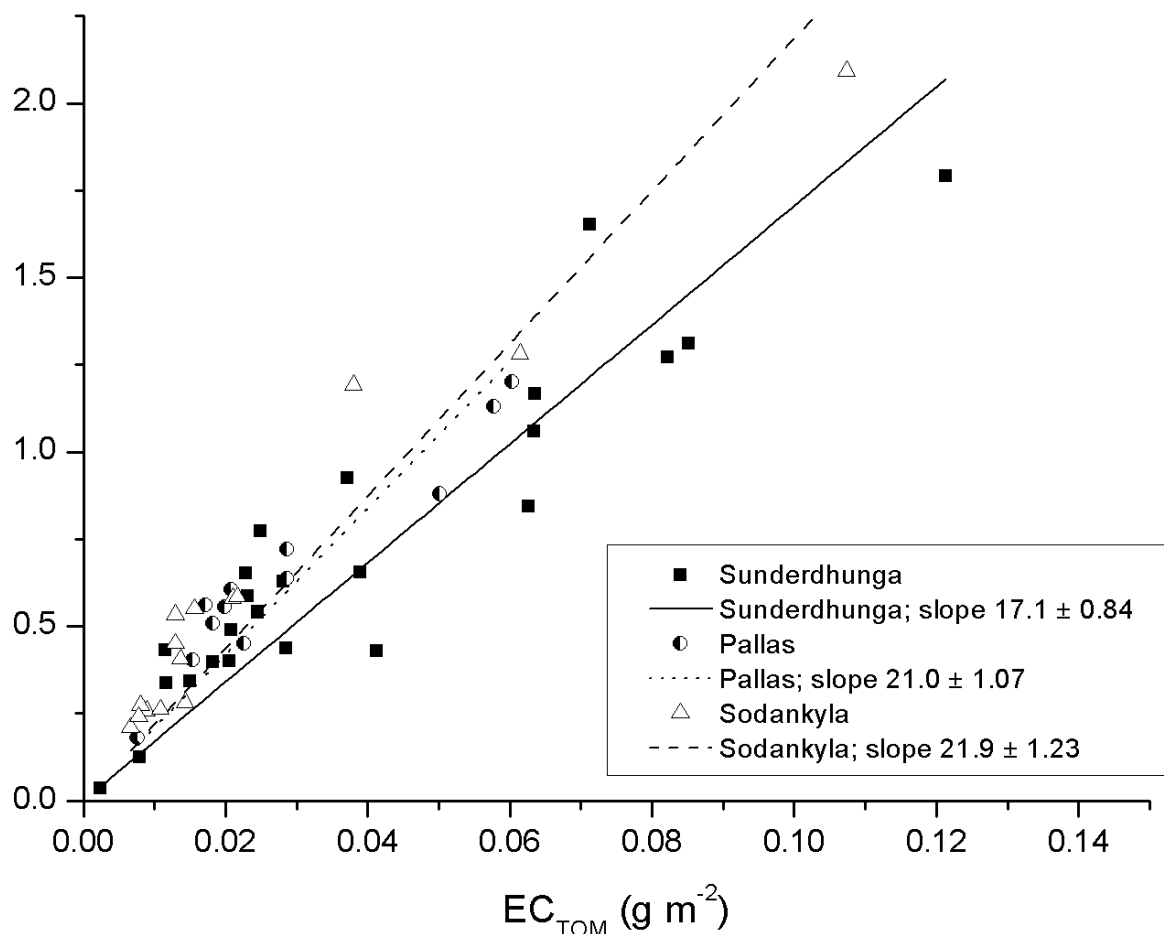
3   _______________________________________

4   Figure 9. The optical depth τ_{EC} as function of the analyzed EC based on TOM, for the Arctic and

5   Himalayan samples.

6   In our case, if the laboratory generated BC consist of smaller particles compared to the snow samples

7   this could lead to a larger MAC value for the lab-standards. The size distribution of the BC particles in

8   the filters are unknown to us, but as suggested by the modelled MAC curve, presented in Figure 10, this

9   size dependence can play a role. The modelled MAC for theoretical BC particles demonstrates a

10   decrease in MAC with particle size, particularly for particles larger than about 130 nm. The absorption

11   efficiencies were calculated for $\lambda = 526$ nm by using the Mie code of Barber and Hill (1990) and for

12   BC we use the same complex refractive index of 1.85 - 0.71i that was used by Lack and Cappa (2010)

13   and a particle density of 1.7 g cm^{-3}.
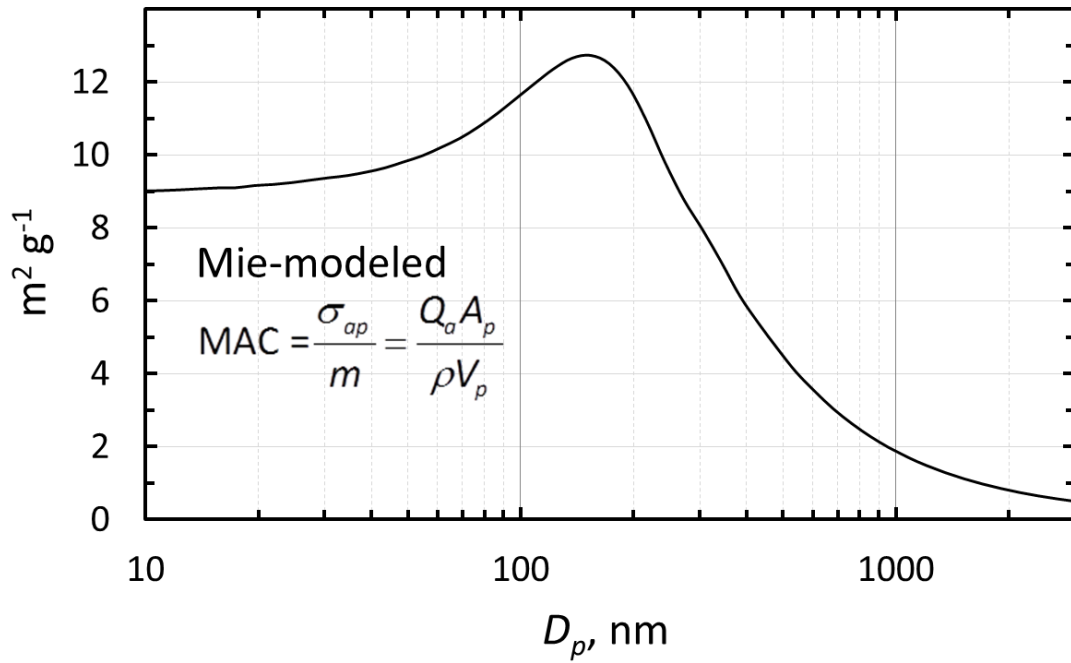
2   Figure 10. Modeled mass absorption coefficient (MAC) of single BC particles as a function of particle

3   diameter at $\lambda = 526$ nm.

4   Another hypothesis is related to the fact that the samples are liquids and that the matrix is strongly light

5   scattering and rather thick. It is likely that the liquid will embed the particles deeper into the filter than

6   what is typical for air samples (e.g. Chen et al., 2004). In air and on filter surfaces, BC mixed with a

7   scattering medium shows enhanced absorption. On the samples presented in Table 1, about 90 to 95%

8   of the carbon is water insoluble organic carbon, whereas the laboratory BC was essentially free from

9   OC. This difference could explain the lower MAC for the ambient samples if the net effect of the added

10   OC actually made the BC less efficient absorber in this particular matrix. Further tests are required,

11   however, to confirm this hypothesis.

12   *3.2.2 Dust fraction of LAI in snow*

13   Because the ambient mineral dust MAC value is unknown for our snow samples, it is not possible to

14   use the SiC or stone crush MAC values to estimate the dust content on the filters. Instead, we use the

15   fraction of minerals (f_D) expressed in percent of the total optical thickness, $\left(\frac{\tau_D}{\tau_{TOT}} \, 100\, \% \right)$ to estimate

16   the mineral aerosol contribution to the filter absorption (at $\lambda = 526$ nm). In our data set, there is a

17   systematic difference between the two Arctic sites and the Himalaya site (Fig. 11). For Pallas and

18   Sodankylä f_D is typically less than 20 %, whereas for Sunderdhunga f_D is typically much greater than

19   that, with modes at 35 and 65 %. For the Arctic, the values are broadly in line with previous estimates

20   on the amount of light absorption caused by LAI other than BC, i.e. 30-50 % (e.g. Doherty et al., 2010).

1   Studies from the Nepalese Himalaya concluded that dust may be responsible for about 40 % of the snow

2   albedo reduction (Kaspari et al., 2014). Similarly, Qu et al. (2014) observed that the contribution of dust

3   to albedo reduction can reach as much as 56 % on a glacier in the Tibetan plateau. Our dust estimate,

4   as a fraction of the optical depth of LAI on the filter, shows similar results or an even greater fraction

5   of dust than these previous studies, highlighting the importance of dust (see also Fig. 12A) causing

6   albedo reduction in this region of the Himalaya.
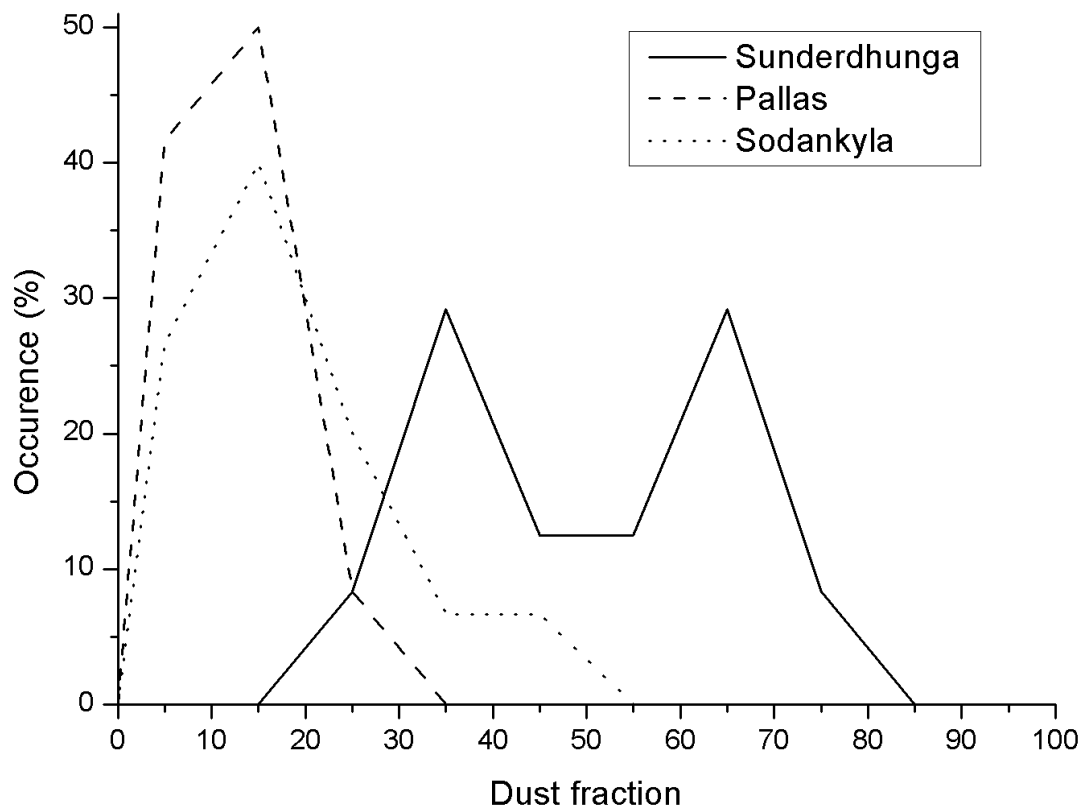
8   Figure 11. Frequency of the occurrence of dust optical thickness fractions at the three sampling sites

9   *3.2.3   Vertical distribution of LAI in Sunderdhunga*

10   An average of the vertical profiles from pits C, D, and E are presented for EC and f_D in Figure 12A.
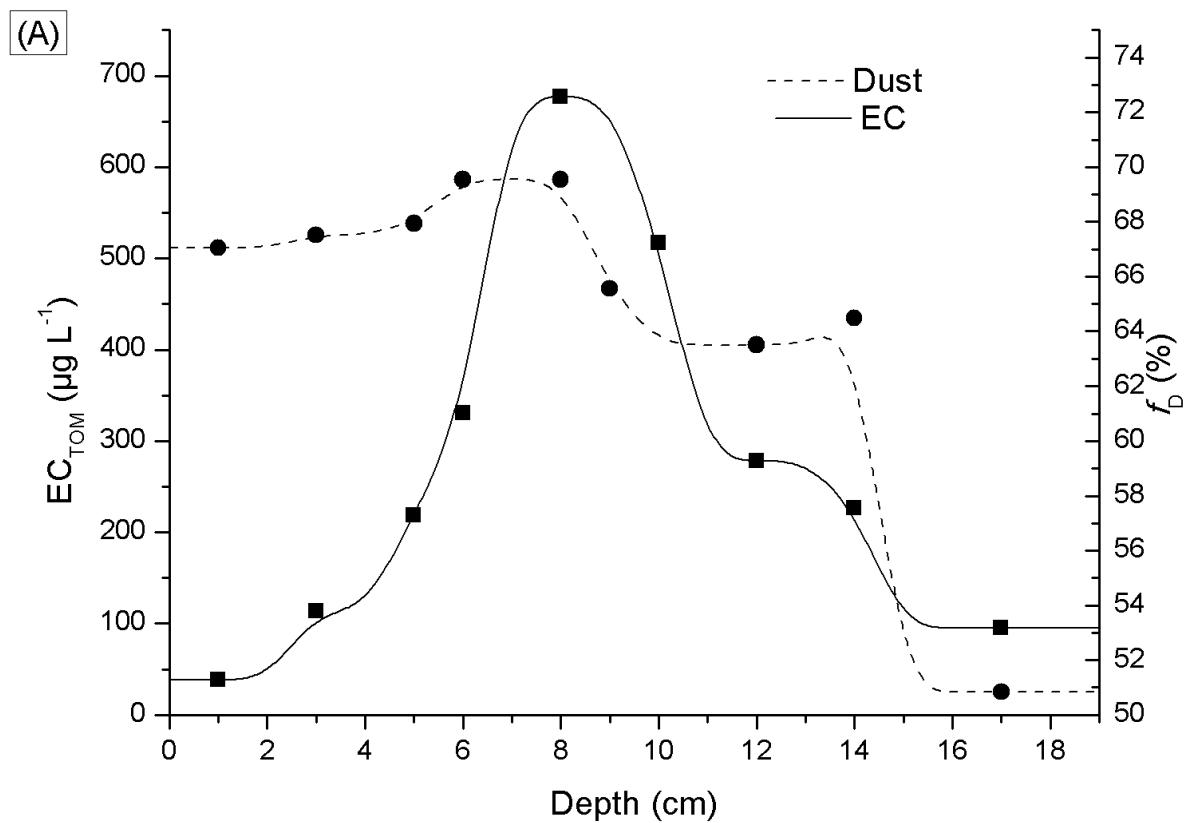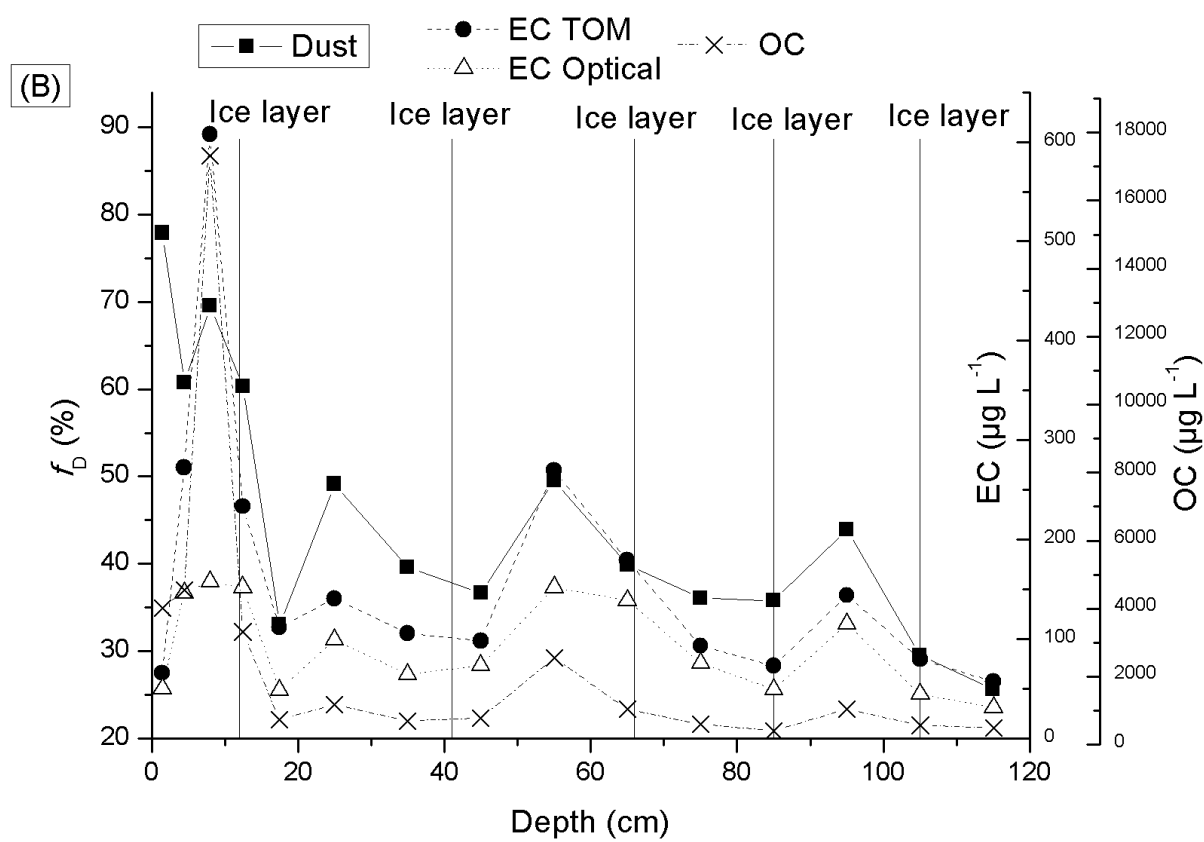
1   Figure 12. (A) Profile displaying average EC concentration and dust fraction from snow pits C and D

2   (Durga Kot glacier), and snow pit E (Bhanolti glacier); (B) Complete vertical profile E, taken at

3   Bhanolti glacier.

4   The variables plotted in Figure 12B display layers of enhanced amounts of both dust and EC, located

5   between ice layers, and additionally high values at the top of the pit above the first ice layer. These

6   layers are interpreted as indicators for seasonal variation at this location, with alternating melt and

7   refreezing periods marked by the ice layers. Since the ice layers and the enhancements in LAI are

8   interleaved it suggest that the impurities were deposited on the glacier mainly in-between the melt and

9   refreeze periods. In addition, the melting seems to take place in a relative shallow layer at the surface

10   and does not protrude deeply, which may cause the annual layers to mix (Doherty et al., 2013). The

11   observed variation in EC and dust values could correspond to the findings of Ginot et al. (2014) and

12   Kaspari et al. (2014) who showed annually peaking BC concentrations in the pre-monsoon in

13   Himalayan ice cores. However, for instance, between the ice layers at ca. 65 and 85 cm, no clear peak

14   is observed in EC or dust values (Fig. 12B), which could either indicate that no peak occurred during

15   that particular year, or an ice layer formed at ca. 65 cm in the middle of the year, similarly as potentially

16   at ca. 105 cm.

17   The snow pit covers potentially five years of snow accumulation which is certainly a too short time

18   period to make any conclusions on a temporal trend of LAI variations at the site. However, an evident

19   increase in LAI is present, especially in the top 20 cm. Due to the time span of the snow pit we cannot

20   know for certain whether this increase presents a short term pollution event or indicates increasing LAI

21   at the site over a longer time period. We have two hypothesis for the observed increase in EC

22   concentrations and the fraction of dust occurring in the top layer of the snow pit. The higher values may

23   be a consequence of increased ambient EC and dust concentrations in the area, causing increased dry

24   and wet deposition fluxes of these impurities to the glacier, even when assuming constant precipitation.

25   Moreover, as it is f_D that increases, the deposition of dust would have had to increase proportionally

26   more than EC and OC. This could be a result from larger areas in the region being free of snow or

27   changes in the wind characteristics (e.g. stronger winds and/or change in direction). On the other hand,

28   local changes in the net snow mass balance due to a larger fraction of the snow being sublimated in the

29   time period covered by the top 20 cm in comparison to the deeper layers, may partly explain the

30   increased EC and dust absorption values at the top of the pit. Both these basic scenarios can be in effect

31   at the same time.

32   Interestingly, while the EC and OC concentrations and f_D are peaking at the top of the snow pit and

33   potentially decrease very slightly towards the bottom of the snow pit, the absorbing efficiency of EC

34   seems to be decrease towards the top of the snow pit. We illustrate this in Figure 13 by plotting the ratio

35   between the optical EC from the OCEC-analyzer and the analyzed EC based on TOM, and scale this

1   ratio with the MAC value of 39.8 derived in Figure 3. While the EC concentrations in the snow are the

2   highest at the top of the pit, it appears that at the same time this EC is a less potent light absorber per

3   unit mass (Fig. 13) than in deeper snow layers. This observation is rather hypothetical, and it needs to

4   be further explored.
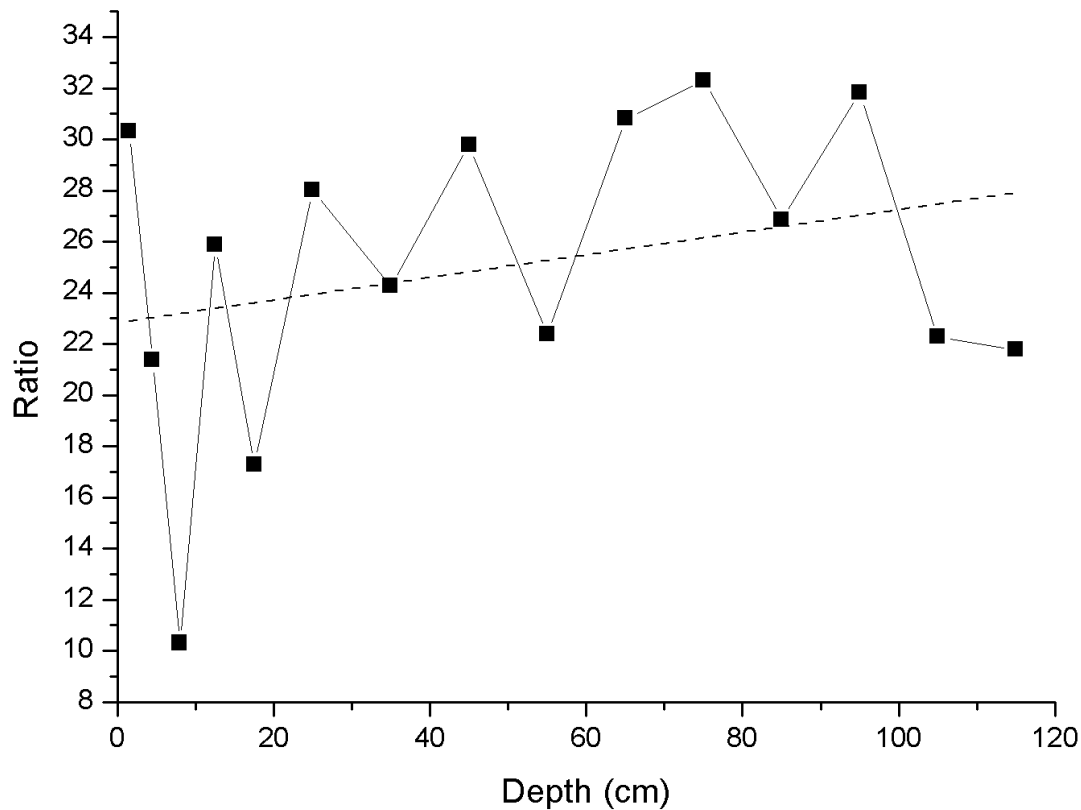
6   Figure 13. The ratio between the optical EC content and analyzed EC content (TOM method) as

7   measured by the OCEC-analyzer using the EUSAAR-2 thermal protocol. The ratio is scaled by the

8   effective MAC value of 39.78 m^2 g^{-1} derived in Figure 3.

9   **4. Conclusions**

10   Here, first observations of LAI in snow originating from two glaciers in the Indian Himalaya are

11   presented with a method not used widely before to determine LAI in snow. Consisting of a custom built

12   PSAP and an OCEC-analyzer, the attenuation of light is studied on quartz filters, providing estimates

13   on the fraction of light-absorbance caused by non-EC constituents in LAI. Himalayan data display a

14   much greater light-absorbance by dust in the LAI compared to filter samples originating from the

15   seasonal snowpack of Arctic Finland. The role of dust in reducing the snow albedo in this part of

16   Himalayan glaciers needs to be further evaluated, as our results suggest that it might be the dominating

17   LAI in the snow. Our measurements further reveal that the optical properties of EC are different for

18   laboratory generated soot compared to EC deposited on snow. Our finding of a MAC value of about

1   half of the laboratory EC for the ambient EC particles, ~~it~~ can have implications for the snow albedo

2   reduction caused by EC. Over the last approximately five year period in the Himalaya, EC

3   concentrations in the snow display signs of increase in the top part of the snow pit compared to deeper

4   layers, while at the same time its light absorbing potential suggests a decrease towards the highest EC-

5   laden layers. Consequently, additional work on the optical properties of EC in snow are needed to enable

6   more accurate estimates of albedo reduction caused by EC in snow, both spatially and temporally. This

7   should be done by measuring the EC particles light-absorption properties while in the snow since the

8   ambient conditions can be different than laboratory settings.

9   **Acknowledgments**

10   This work has been supported by the Academy of Finland projects: Absorbing Aerosols and Fate of

11   Indian Glaciers (AAFIG; project number 268004) and Greenhouse gas, aerosol and albedo variations

12   in the changing Arctic" (project number 269095). The Academy of Finland Center of Excellence

13   program (project number 272041), as well as the Nordic research and innovation initiative Cryosphere-

14   Atmosphere Interactions in a Changing Arctic Climate have also supported this work. Jonas Svensson

15   is thankful for the support from Svenska kulturfonden. We would like to thank the providers of the soot

16   Consti Taloteknikka, and Göran Lidén at SU luftlab for the mineral samples. The ACES department at

17   Stockholm University, is part of the Bolin centre for climate research. Finally we would like to thank

18   the participants of the AAFIG 2015 expedition, including Sherpas and guides from Real adventure, for

19   their work during the expedition.

20   **References**

21   AMAP: The Impact of Black Carbon on Arctic Climate. Arctic Monitoring and Assessment Programme
22   (AMAP), Oslo, Norway, 72 pp, 2011.
23   Aoki, T., Motoyoshi, H., Kodama, Y., Yasunari, T. J., Sugiura, K., and Kobayashi, H.: Atmospheric
24   aerosol deposition on snow surfaces and its effect on albedo. SOLA, 2, 13–16, doi: 10.2151/sola.2006-
25   004, 2006.
26   Barber, P. W. and Hill, S. C.: Light scattering by particles: Computational methods, World Scientific
27   Publishing, Singapore, 1990.
28   Birch, M. E., and Cary R. A.: Elemental carbon-based method for monitoring occupational exposures,
29   to particulate diesel exhaust, Aerosol. Sci. Technol., 25, 221– 241, 1996.
30   Bolch, T., Kulkarni, A., Kääb, A., Huggel, C., Paul, F., Cogley, J. G., Frey, H., Kargel, J. S., Fujita, K.,
31   Scheel, M., Bajracharya, S., and Stoffel, M.: The State and Fate of Himalayan Glaciers, Science, 336,
32   310–314, doi:10.1126/science.1215828, 2012.
33   Bond, T. C., Anderson, T. L., and Campbell, D.: Calibration and Intercomparison of Filter-Based
34   Measurements of Visible Light Absorption by Aerosols, Aerosol Sci. Technol. 30:582–600, 1999.
35   Bond, T. C., Doherty, S. J., Fahey, D. W., Forster, P. M., Berntsen, T., DeAngelo, B. J., Flanner, M. G,
36   Ghan, S., Kärcher, B., Koch, D., Kinne, S., Kondo, Y., Quinn, P. K., Sarofim, M. F., Schultz, M. G.,
37   Schulz, M., Venkataraman, C., Zhang, H., Zhang, S., Bellouin, N., Guttikunda, S. K., Hopke, P. K.,
38   Jacobson, M. Z., Kaiser, J. W., Klimont, Z., Lohmann, U., Schwarz, J. P., Shindell, D., Storelvmo, T.,
39   Warren, S. G., and Zender, C.S.: Bounding the role of black carbon in the climate system: A scientific
40   assessment, J. Geophys. Res. Atmos., 188, 5380–5552, doi: 10.1002/jgrd.50171, 2013.

1 Bond, T., Bhardwaj, E., Dong, R., Jogani, R., Jung, S., Roden, C., Streets, D. G., and Trautmann, N.:
2 Historical emissions of black and organic carbon aerosol from energy-related combustion, 1850–2000,
3 Global Biogeochem. Cy., 21, doi:10.1029/2006GB002840, 2007.
4 Cachier, H., Bremond, M.P., and Buat-Ménard, P.: Determination of atmospheric soot carbon with a
5 simple thermal method, Tellus Ser.B, 41B, 379-390, 1989.
6 Cappa, C., Onasch, T., Massoli, P., Worsnop, D., Bates, T., Cross, E., Davidovits, P., Hakala, J.,
7 Hayden, K., Jobson, B., Kolesar, K., Lack, D., Lerner, B., Li, S., Mellon, D., Nuaaman, I., Olfert, J.,
8 Petäja, T., Quinn, P., Song, C., Subramanian, R., Williams, E., and Zaveri, R.: Radiative absorption
9 enhancements due to the mixing state of atmospheric black carbon, Science, 337, 1078–1081,
10 doi:10.1126/science.1223447, 2012.
11 Cavalli, F., Viana, M., Yttri, K.E., Genberg, J., and Putaud, J-P.: Toward a standardised thermal-optical
12 protocol for measuring atmospheric organic and elemental carbon: the EUSAAR protocol, Atmos.
13 Meas. Tech. 3, 79–89, doi:10.5194/amt-3-79-2010, 2010.
14 Chen, L.-W. A., Chow, J. C., Watson, J. G., Moosmüller, H., and Arnott, W. P.: Modeling reflectance
15 and transmittance of quartz-fiber filter samples containing elemental carbon particles: Implications for
16 thermal/optical analysis, J. Aerosol Sci., 35, 765–780, 2004.
17 Chow, J. C., & Watson, J. G.: PM2:5 carbonate concentrations at regionally representative Interagency
18 monitoring of protected visual environment sites. J. Geophys. Res., 107(D21), 8344,
19 doi:10.1029/2001JD000574, 2002.
20 Collaud Coen, M., Weingartner, E., Apituley, A., Ceburnis, D., Fierz-Schmidhauser, R., Flentje, H.,
21 Henzing, J. S., Jennings, S. G., Moerman, M., Petzold, A., Schmid, O. and Baltensperger, U.:
22 Minimizing light absorption measurement artifacts of the Aethalometer: evaluation of five correction
23 algorithms, Atmos. Meas. Tech., 3, 457–474, 10.5194/amt-3-457-2010, 2010.
24 Doherty, S. J., Warren, S. G., Grenfell, T. C., Clarke, A. D., and Brandt, R. E.: Light-absorbing
25 impurities in Arctic snow, Atmos. Chem. Phys., 10, 11647–11680, doi: 10.5194/acp-10-11647-2010,
26 2010.
27 Doherty, S. J., Grenfell, T. C., Forsström, S., Hegg, D. L., Brandt, R. E., and Warren, S. G.: Observed
28 vertical redistribution of black carbon and other insoluble light-absorbing particles in melting snow, J.
29 Geophys. Res., 118, 1–17, doi:10.1002/jgrd.50235, 2013.
30 Doherty, S. J., D. A. Hegg, J. E. Johnson, P. K. Quinn, J. P. Schwarz, C. Dang, and Warren, S.G.:
31 Causes of variability in light absorption by particles in snow at sites in Idaho and Utah, J. Geophys.
32 Res. Atmos., 121, 4751-4768, doi:10.1002/2015JD024375, 2016.
33 Dumont, M., Brun, E., Picard, G., Michou, M., Libois, Q., Petit, J.-R., Geyer, M., Morin, S., and Josse,
34 B.: Contribution of light-absorbing impurities in snow to Greenland's darkening since 2009, Nat.
35 Geosci., 7, 509–512, doi:10.1038/ngeo2180, 2014.
36 Forsström, S., Ström, J., Pedersen, C. A., Isaksson, E., and Gerland, S.: Elemental carbon distribution
37 in Svalbard snow, J. Geophys. Res. Atmos., 114, D19112, doi:10.1029/2008JD011480, 2009.
38 Forsström, S., Isaksson, E., Skeie, R. B., Ström, J., Pedersen, C. A., Hudson, S. R., Berntsen, T. K.,
39 Lihavainen, H., Godtliebsen, F., and Gerland, S.: Elemental carbon measurements in European Arctic
40 snow packs, J. Geophys. Res. Atmos., 118, 13614–13627, doi:10.1002/2013JD019886, 2013.
41 Gautam R., Hsu, N. C., Lau, W. K.-M., and T. J. Yasunari, T. J.: Satellite observations of desert dust-
42 induced Himalayan snow darkening, Geophys. Res. Lett., 40, 988–993, doi:10.1002/grl.50226, 2013.
43 Gertler, C.G., Puppala, S.P., Panday, A., Stumm, D., Shea, J.: Black carbon and the Himalayan
44 cryosphere: a review. Atmos. Environ. 125, 404–417, doi.org/10.1016/j.atmosenv.2015.08.078, 2016.
45 Ginot, P., Dumont, M., Lim, S., Patris, N., Taupin, J.-D., Wagnon, P., Gilbert, A., Arnaud, Y., Marinoni,
46 A., Bonasoni, P., and Laj, P.: A 10 year record of black carbon and dust from a Mera Peak ice core
47 (Nepal): variability and potential impact on melting of Himalayan glaciers, The Cryosphere, 8, 1479–
48 1496, doi:10.5194/tc-8-1479-2014, 2014.
49 Grenfell, T. C., Doherty, S. J., Clarke, A. D., and Warren, S. G.: Spectrophotometric determination of
50 absorptive impurities in snow, Appl. Opt., 50(14), 2037–2048.
51 Hagler, G. S. W., Bergin, M. H., Smith, E. A., Dibb, J. E., Anderson, C., and Steig, E. J.: Particulate
52 and water-soluble carbon measured in recent snow at Summit, Greenland, Geophys. Res. Lett., 34,
53 L16505, doi:10.1029/2007GL030110, 2007.

1   Hansen, A.D. A., Kapustin, V. N., Kopeikin, V. M., Gillette, D. A., and Bodhaine, B. A.: Optical
2   absorption by aerosol black carbon and dust in a desert region of central Asia, Atmos. Environ., Part ,4,
3   27,4, 2527-2531, 1993
4   Hinds,W. C.: Aerosol Technology,Wiley-interscience, 1999.
5   Hyvärinen, A.-P., Raatikainen, T., Brus, D., Komppula, M., Panwar, T. S., Hooda, R. K., Sharma, V.
6   P., and Lihavainen, H.: Effect of the summer monsoon on aerosols at two measurement stations in
7   Northern India – Part 1: PM and BC concentrations, Atmos. Chem. Phys., 11, 8271-8282,
8   doi:10.5194/acp-11-8271-2011, 2011.
9   Immerzeel, W. W., van Beek, L. P. H., and Bierkens, M. F. P.: Climate Change Will Affect the Asian
10 Water Towers, Science, 328, 1382–1385, doi:10.1126/science.1183188, 2010.
11 Kaspari, S., Painter, T. H., Gysel, M., Skiles, S. M., and Schwikowski, M.: Seasonal and elevational
12 variations of black carbon and dust in snow and ice in the Solu-Khumbu, Nepal and estimated radiative
13 forcings, Atmos. Chem. Phys., 14, 8089–8103, doi:10.5194/acp-14-8089-2014, 2014.
14 Kääb, A., Berthier, E., Nuth, C., Gardelle, J., and Arnaud, Y.: Contrasting patterns of early 21st century
15 glacier mass change in the Himalaya, Nature, 488, 495–498, doi:10.1038/nature11324, 2012.
16 Krecl, P., Ström, J., and Johansson, C.: Carbon content of atmospheric aerosols in a residential area
17 during the wood combustion season in Sweden, Atmos. Environ., 41, 6974–6985, 2007.
18 Lack, D. A. and Cappa, C. D.: Impact of brown and clear carbon on light absorption enhancement,
19 single scatter albedo and absorption wavelength dependence of black carbon, Atmos. Chem. Phys., 10,
20 4207-4220, doi:10.5194/acp-10-4207-2010, 2010.
21 Lavanchy, V. M. H., Gäggler, H. W., Schotterer, U., Schwikowski, M., and Baltensperger, U.:
22 Historical record of carbonaceous particle concentrations from a European high-alpine glacier (Colle
23 Gnifetti, Switzerland), J. Geophys. Res., 104, 21227–21236, doi:10.1029/1999JD900408, 1999.
24 Lim, S., Faïn, X., Zanatta, M., Cozic, J., Jaffrezo, J.-L., Ginot, P., and Laj, P.: Refractory black carbon
25 mass concentrations in snow and ice: method evaluation and inter-comparison with elemental carbon
26 measurement, Atmos. Meas. Tech., 7, 3307-3324, doi:10.5194/amt-7-3307-2014.
27 Lutz, S., Anesio, A.M., Raiswell, R., Edwards, A., Newton, R.J., Gill, F., and Benning, L.G.: The
28 biogeography of red snow microbiomes and their role in melting arctic glaciers. Nat. Commun. 7:
29 11968, doi: 10.1038/ncomms11968, 2016.
30 Meinander, O., Kazadzis, S., Arola, A., Riihelä, A., Räisänen, P., Kivi, R., Kontu, A., Kouznetsov, R.,
31 Sofiev, M., Svensson, J., Suokanerva, H., Aaltonen, V., Manninen, T., Roujean, J.-L., and Hautecoeur,
32 O.: Spectral albedo of seasonal snow during intensive melt period at Sodankylä, beyond the Arctic
33 Circle, Atmos. Chem. Phys., 13, 3793-3810, doi:10.5194/acp-13-3793-2013, 2013.
34 McConnell, J. R., Edwards, R., Kok, G. L., Flanner, M. G., Zender, C. S., Saltzman, E. S., Banta, J. R.,
35 Pasteris, D. R., Carter, M. M., and Kahl, J. D. W.: 20th century industrial black carbon emissions altered
36 arctic climate forcing, Science, 317, 1381–1384, doi:10.1126/science.1144856, 2007.
37 Ming, J., Cachier, H., Xiao, C., Qin, D., Kang, S., Hou, S., and Xu, J.: Black carbon record based on a
38 shallow Himalayan ice core and its climatic implications, Atmos. Chem. Phys., 8, 1343– 1352,
39 doi:10.5194/acp-8-1343-2008, 2008.
40 Ming, J., Xiao, C., Du, Z., and Yang, X.: An Overview of Black Carbon Deposition in High Asia
41 Glaciers and its Impacts on Radiation Balance, Adv.Water Resour., 55, 80–87, 2013.
42 Ming, J., Wang, Y., Du, Z., Zhang, T., Guo, W., Xiao, C., Xu, X., Ding, M., Zhang, D., and Yang,
43 W.: Widespread albedo decreasing and induced melting of Himalayan snow and ice in the early 21st
44 century. PLoS One 10(6):e0126235. doi:10.1371/journal.pone.0126235, 2015.
45 Painter, T. H., Barrett, A. P., Landry, C. C., Neff, J. C., Cassidy, M. P., Lawrence, C. R., McBride, K.
46 E., and Farmer, G. L.: Impact of disturbed desert soils on duration of mountain snow cover, Geophys.
47 Res. Lett., 34, L12502, doi:10.1029/2007GL030284, 2007.
48 Painter, T. H., Skiles, S. M., Deems, J. S., Bryant, A. C., and Landry C.C.: Dust radiative forcing in
49 snow of the Upper Colorado River Basin: 1. A 6 year record of energy balance, radiation, and dust
50 concentrations. Water Resources Research, 48, doi: 10.1029/2012wr011985, 2012.
51 Qian,Y., Yasunari, T. J., Doherty, S. J., Flanner, M. G., Lau, W. K., Ming, J., Zhang, R.: Light-
52 absorbing particles in snow and ice: measurement and modeling of climatic and hydrological impact.
53 Adv. Atmos. Sci. 32(1),64–91, doi: 10.1007/s00376-014-0010-0, 2015.

1   Qu, B., Ming, J., Kang, S.-C., Zhang, G.-S., Li, Y.-W., Li, C.-D., Zhao, S.-Y., Ji, Z.-M., and Cao, J.-J.:
2   The decreasing albedo of the Zhadang glacier on western Nyainqentanglha and the role of light-
3   absorbing impurities, Atmos. Chem. Phys., 14, 11117-11128, doi:10.5194/acp-14-11117-2014, 2014.
4   Ruppel, M. M., Isaksson, E., Ström, J., Beaudon, E., Svensson, J., Pedersen, C. A., and Korhola, A.:
5   Increase in elemental carbon values between 1970 and 2004 observed in a 300-year ice core from
6   Holtedahlfonna (Svalbard), Atmos. Chem. Phys., 14, 11447-11469, doi:10.5194/acp-14-11447-2014,
7   2014.
8   Raatikainen, T., Brus, D., Hooda, R. K., Hyvärinen, A.-P., Asmi, E., Sharma, V. P., Arola, A., and
9   Lihavainen, H.: Size-selected black carbon mass distributions and mixing state in polluted and clean
10 environments of northern India, Atmos. Chem. Phys., 17, 371-383, doi:10.5194/acp-17-371-2017,
11 2017.
12 Schmitt, C. G., All, J. D., Schwarz, J. P., Arnott, W. P., Cole, R. J., Lapham, E., and Celestian, A.:
13 Measurements of light-absorbing particles on the glaciers in the Cordillera Blanca, Peru, The
14 Cryosphere, 9, 331-340, doi:10.5194/tc-9-331-2015, 2015.
15 Schwarz, J. P., Doherty, S. J., Li, F., Ruggiero, S. T., Tanner, C. E., Perring, A. E., Gao, R. S., and
16 Fahey, D. W.: Assessing Single Particle Soot Photometer and Integrating Sphere/Integrating Sandwich
17 Spectrophotometer measurement techniques for quantifying black carbon concentration in snow,
18 Atmos. Meas. Tech., 5, 2581–2592, doi:10.5194/amt-5-2581-2012, 2012.
19 Schwarz, J. P., Gao, R. S., Perring, A. E., Spackman, J. R., and Fahey, D.W.: Black carbon aerosol size
20 in snow, Nat. Sci. Reports, 3, 1356, doi:10.1038/srep01356, 2013.
21 Shindell, D., Kuylenstierna, J. C. I., Vignati, E., van Dingenen, R., Amann, M., Klimont, Z., Anenberg,
22 S. C., Muller, N., JanssensMaenhout, G., Raes, F., Schwartz, J., Faluvegi, G., Pozzoli, L., Kupiainen,
23 K., Höglund-Isaksson, L., Emberson, L., Streets, D., Ramanathan, V., Hicks, K., Oanh, N. T. K., Milly,
24 G., Williams, M., Demkine, V., and Fowler, D.: Simultaneously Mitigating Near-Term Climate Change
25 and Improving Human Health and Food Security, Science, 335, 183–189, doi:
26 10.1126/science.1210026, 2012.
27 Svensson, J. Ström, J., Hansson, M., Lihavainen, H., and Kerminen, V.-M.: Observed metre scale
28 horizontal variability of elemental carbon in surface snow, Environ. Res. Lett., 8, 034012,
29 doi:10.1088/1748-9326/8/3/034012, 2013.
30 Svensson J., Virkkula A., Meinander O., Kivekäs N., Hannula H.-R., Järvinen O., Peltoniemi J.I.,
31 Gritsevich M., Heikkilä A., Kontu A., Neitola K., Brus D., Dagsson-Waldhauserova P., Anttila K.,
32 Vehkamäki M., Hienola A., de Leeuw G. & Lihavainen H. 2016: Soot-doped natural snow and its
33 albedo — results from field experiments. Boreal Env. Res. 21: 481–503.
34 Thevenon, F., Anselmetti, F. S., Bernasconi, S. M., and Schwikowski, M.: Mineral dust and elemental
35 black carbon records from an Alpine ice core (Colle Gnifetti glacier) over the last millennium, J.
36 Geophys. Res., 114, 102, doi: 10.1029/2008JD011490, 2009.
37 Virkkula, A., Ahlquist, N. C., Covert, D. S., Arnott,W. P., Sheridan, P. J., Quinn, P. K., and Coffman,
38 D. J. (2005). Modification, Calibration and a Field Test of an Instrument for Measuring Light
39 Absorption by Particles, Aerosol Sci. Technol. 39:68–83.
40 Warren, S. G., and Wiscombe, W. J.: A model for the spectral albedo of snow. II: Snow containing
41 atmospheric aerosols, J. Atmos. Sci., 37, 2734–2745, 1980.
42 Wang, M., Xu, B., Zhao, H., Cao, J., Joswiak, D., Wu, G., and Lin, S.: The Influence of Dust on
43 Quantitative Measurements of Black Carbon in Ice and Snow when Using a Thermal Optical Method,
44 Aerosol Sci. Technol., 46, 60–69, doi:10.1080/02786826.2011.605815, 2012.
45 Xu, B., Yao, T., Liu, X., and Wang, N.: Elemental and organic carbon measurements with a two-step
46 heating-gas chromatography system in snow samples from the Tibetan Plateau, Ann. Glaciol., 43, 257–
47 262, 2006.
48 Xu, B., Cao, J., Hansen, J., Yao, T., Joswiak, D.R., Wang, N., Wu, G., Wang, M., Zhao, H., Yang, W.,
49 Liu, X., and He, J.: Black soot and the survival of Tibetan glaciers. Proc. Nat. Acad. Sci. USA, 106,
50 22114–22118, doi:10.1073/pnas.0910444106, 2009.
51 Yang, S., Xu, B., Cao, J., Zender, C. S., and Wang, M.: Climate effect of black carbon aerosol in a
52 Tibetan Plateau glacier, Atmos. Environ., 111, 71–78, doi.org/10.1016/j.atmosenv.2015.03.016 1352-
53 2310, 2015.
54 Zhang, Y., Kang, S., Li, C., Gao, T., Cong, Z., Sprenger, M., Liu, Y., Li, X,., Guo, J., Sillanpää, M.,
55 Wang, K., Chen, J., Li, Y., Sun, S.: Characteristics of black carbon in snow from Laohugou No. 12

1   glacier on the northern Tibetan Plateau, Sci. Tot. Environ., 607-608, 1237-1249,
2   doi.org/10.1016/j.scitotenv.2017.07.100, 2017.

1 Table 1. Snow pit filter samples from Sunderdhunga 2015. Durga kot glacier snow pits are A-D and Bhanolti glacier snow pit E.

Snow pit ID and elevation (m a.s.l.)	Sample interval (cm)	τTOT	τD	τEC	EC TOM (g m^{-2})	EC optical (g m^{-2})	eEC (g m^{-2})	Total C (g m^{-2})	EC (µg L^{-1})	F$_D$
A, 4869	0-2	3.94	2.63	1.31	0.09	0.05	0.03	1.75	362.18	66.68
	2-5	-	-	-	0.25	0.00	-	0.25	1010.62	-
	5-10	-	-	-	0.30	0.01	-	11.11	1030.84	-
B, 4921	0-2	0.69	0.26	0.43	0.01	0.01	0.01	0.15	40.33	37.64
	2-6	-	4.79	-	0.13	0.04	-	4.24	398.60	-
C, 4921	0-3	0.29	0.16	0.13	0.01	0.00	0.00	0.21	35.71	56.62
	3-6	1.76	1.32	0.44	0.03	0.02	0.01	1.24	55.15	75.12
	6-9	-	5.19	-	0.15	0.00	-	4.88	1095.79	-
	9-13	2.20	1.35	0.84	0.06	0.03	0.02	0.76	381.63	61.57
D, 4950	0-5	0.11	0.07	0.04	0.00	0.00	0.00	0.06	13.20	66.65
	5-10	-	-	-	0.07	0.01	-	6.70	327.14	-
	10-20	1.37	0.94	0.43	0.04	0.02	0.01	0.64	220.21	68.63
	20-30	1.15	0.66	0.49	0.02	0.02	0.01	0.34	78.58	57.36
E, 5008	0-3	1.81	1.41	0.40	0.02	0.02	0.01	1.27	65.73	77.87
	3-6	3.25	1.97	1.27	0.08	0.04	0.03	1.45	272.57	60.77
	6-10	5.88	4.09	1.79	0.12	0.03	0.05	3.58	607.83	69.55
	10-15	2.94	1.77	1.17	0.06	0.04	0.03	0.97	233.21	60.32
	15-20	0.98	0.32	0.66	0.04	0.02	0.02	0.30	111.42	33.05
	20-30	1.06	0.52	0.54	0.02	0.02	0.01	0.23	140.71	49.15
	30-40	1.04	0.41	0.63	0.03	0.02	0.02	0.21	105.55	39.61
	40-50	1.03	0.38	0.65	0.02	0.02	0.02	0.21	98.15	36.71
	50-60	2.10	1.04	1.06	0.06	0.04	0.03	0.66	269.67	49.53
	60-70	2.75	1.10	1.65	0.07	0.06	0.04	0.49	179.30	39.90
	70-80	1.21	0.44	0.77	0.02	0.02	0.02	0.19	93.00	36.12
	80-90	0.91	0.33	0.59	0.02	0.02	0.01	0.15	72.80	35.81

90-100	1.65	0.73	0.92	0.04	0.03	0.02	0.31	143.80	43.95
100-110	0.57	0.17	0.40	0.02	0.01	0.01	0.15	79.31	29.54
110-120	0.46	0.12	0.34	0.02	0.01	0.01	0.15	56.91	25.68